DEVELOPMENT OF A MICROINJECTION PLATFORM FOR THE EXAMINATION OF HOST-BIOMATERIAL INTERACTIONS IN ZEBRAFISH EMBRYOS

by

William Tanaka Park Chaplin

A thesis submitted to the Department of Chemical Engineering

In conformity with the requirements for

the degree of Master of Applied Science

Queen's University

Kingston, Ontario, Canada

(September, 2017)

Abstract

Current approaches in biomaterial development require a series of *in vitro* and *in vivo* assays to identify and optimize candidate materials. Current *in vitro* assays have low labor requirements and are relatively cheap compared to *in vivo* studies but fail to recapitulate the host response. Alternatively, *in vivo* models do not provide a wide array of analytical tools, and are labor intensive. Therefore, a gap exists for a model that retains the low labor requirements and cost of *in vitro* assays, while allowing researchers the ability to observe a true host-biomaterial interaction. Zebrafish have the potential to provide such a model due to their naturally transparency, high fecundity that enables a single female to produce upwards of a hundred eggs a week, and the wide array of transgenic strains.

After establishment of a colony at Queen's University, microinjection techniques were developed to assess the feasibility of using zebrafish as a model for host-biomaterial interaction using poly(styrene) and poly(ethylene) microparticles with diameters of 10, 25, and 50 µm. Implantation success and retention rates were examined, as well as zebrafish mortality rates out to 30 days post injection (dpi). Successful implantation rates were measured at 33%, 17%, and 12% for 10, 25, and 50 µm microparticles, respectively. Retention rates were identical for 10 and 25 µm microparticles at 78%, but implant retention was 11% for 50 µm microparticles. Furthermore, 10 µm microparticles injected with 20 µm bore needles showed no difference in survival from controls. However, 25 µm implants with 50 µm bore sizes, and 50 µm implants with 100 µm bore sizes both showed a reduction in viability post injection in zebrafish compared to tricaine controls. Based on these preliminary results, zebrafish embryos tolerate implants ranging from 10 – 25 µm in diameter, while 50 µm was deemed too large for the embryo. Further refinement of techniques is anticipated to improve success and retention rates.

Histology techniques were developed for use with 3 – 5 mm zebrafish larvae. By embedding tissues in an agar array and reducing fixation times to 2 hours, improvements were observed in tissue cohesion. Additionally, the agar matrix provides a well-organized structure, which lends itself to improved efficiency for future work.

Acknowledgements

I would like to thank the huge number of people who helped me complete this work. These people are not strictly limited to those who helped with lab work, but also those who assisted with my own personal growth, and emotional support through tough times.

First, I would like to thank my supervisor Dr. Lindsay Fitzpatrick, who always ensured that I could keep moving forward, even when the fish had not yet arrived. I would also like to thank my lab mates, Laura McKiel, Rosa Comas, and Emma Henderson, who supported me through good times and bad, and always made sure the work environment was both professional and enjoyable. I would also like to acknowledge Janine Handforth, Andrew Winterborn, and the entire ACC staff that helped me with the colony establishment and maintenance. Furthermore, I would like to acknowledge the support by Lee Boudreau from the Queen's Laboratory for Molecular Pathology, whose histological expertise was invaluable, and without whom I would have taken at least another half year of troubleshooting before finishing the paraffin embedding.

A special thanks to the educators who taught me during my graduate course, Dr. Brian Amsden, Dr. Dominik Barz, Dr. Carlos Escobedo, Dr. Lindsay Fitzpatrick, and Dr. Marianna Kontopoulou, the knowledge I gained in each of your courses guided me through my research, and assisted in the development of several potential ideas.

I would like to acknowledge the continued support of all my friends at Queen's University, some have been with me since day 1 of my undergraduate degree here, and others I've picked up along the way. Without your support, I would not have gotten this far. Finally, I would like to thank my family Dr. William Chaplin, Dr. Karina Davidson, and my sister Merete Chaplin, without whom I would not have decided to follow my dreams, knowing that they would support me no matter where I ended up.

Table of Contents

List of Figures

List of Tables

List of Abbreviations

BSA	Bovine serum albumin
DAPI	4’,6-Diamidino-2-Phenylindole, Dihydrochloride
DPF	Days post fertilization
DPI	Days post injection
ECM	Extracellular matrix
EFW	Endotoxin free water
EU	Endotoxin units
FBGC	Foreign body giant cell
FBR	Foreign body reaction
FGF	Fibroblast growth factor
GFP	Green fluorescent proteins
H&E	Hematoxylin and Eosin
HPI	Hours post injection
IFN	Interferon
IL	Interleukin
KGF	Keratinocyte growth factor
MMP	Metalloproteinases
PDGF	Platelet derived growth factor
PS	Poly(styrene)
PE	Poly(ethylene)
RO	Reverse Osmosis
ROS	Reactive oxygen species
TGF	Transforming growth factor
TNF	Tumor necrosis factor
VEGF	Vascular endothelial growth factor

Chapter 1

Introduction

The National Institute of Health defines a biomaterial as “any substance other than a drug, natural or synthetic, that evaluates, treats, augments, or replaces any tissue, organ, and body function” [1]. With an increasing understanding of polymer chemistry and biology, novel biomaterials are being developed with highly tunable properties that can mimic natural tissues, respond to stimuli, and interact with the patient’s body by enhancing the natural healing response [2-4]. However, prior to implantation in humans, extensive testing is required to assure efficacy and safety of new materials. Material performance *in vivo* and the host response to the material are critical factors in this testing.

Currently, initial material development occurs *in vitro*, during which cell-based assays are frequently used to assess material biocompatibility, and certain application-specific cell-material interactions. These cellular assays often occur in 2D, monolayer cultures within simplistic and relatively controlled microenvironments [5, 6]. Generally, these *in vitro* assays examine one or two cell types simultaneously, and examples of standard assays include cell viability, adhesion and proliferation on material substrates, or the effect of these cells on the biomaterial itself [6-8]. Cell-based assays may also look at application-dependent outcomes, including changes in gene or protein expression, cell differentiation, or enhanced growth of specific cell lines [5, 6, 9].

While *in vitro* assays are often cheaper and faster compared to their *in vivo* counterparts, there are inherent limitations in the ability of these assays to mimic the *in vivo* host response. Upon implantation, materials are exposed to a complex and dynamic environment that consists of extracellular matrix and complex biological fluids that contain a multitude of proteins, lipids, and enzymes, and multiple cell populations that range from fibroblasts and other tissue resident cells to circulating cells of the innate immune system [10, 11]. Furthermore, the *in vivo* environment itself is often hostile, containing elements that can degrade the material [12, 13]. This can affect the stability of the material, and cause deviations from expected degradation rates observed *in vitro* [10, 12]. Materials are evaluated to ensure that they perform their desired role effectively within the *in vivo* environment, in an application-dependent manner. For example, molecule-eluting devices can be implanted subcutaneously to determine release rates, or bone replacements can be tested in critical bone defect models for their ability to regenerate bones [14-16]. One critical biological response, in the context of biomaterials research, is foreign body reaction (FBR) [10]. The FBR is characterized by a chronic inflammatory response at the tissue-material interface that often leads to the eventual fibrotic encapsulation of the offending material [17]. The FBR is a critical factor in the overall performance of a material (or associated device) and may vary in a material and application dependent way [10, 12]. The FBR is a complex series of events involving multiple cell types and a dynamic environment, *in vitro* cell assays cannot accurately recapitulate or predict the host response to the implanted material [17, 18]. Therefore, *in vivo* assays offer insight into how a material would be expected to interact with a human host.

Current *in vivo* assays have significant limitations in the analytical tools available [19]. Typically, analysis of the FBR in rodent models requires end-point methods, such as histology or immunohistochemical staining [16, 20]. Due to the nature of endpoint analysis, time points are often selected prior to the beginning of the trial, which can cause researchers to miss key interactions between the host and material [13, 14, 21]. Furthermore, the number of time points are often limited due to cost, statistical power requirements, and ethical considerations to reduce the number of animals being used [6, 22, 23]. Finally, proper maintenance of the experimental animals can become expensive during long term trials, and the analytical tools themselves are often significantly more expensive than *in vitro* assays [24]. Recent advances in technology, such as intravital imaging and bioluminescence, do provide the potential for real-time analysis, however these new methods are technically challenging and expensive [19, 22]. Thus, there exists a gap between *in vitro* and *in vivo* assays, and new experimental models are needed that retain the complex host microenvironment, while reducing the cost and labour requirements associated with current mammalian animal models.

Zebrafish can offer an intermediate stage between *in vitro* testing and current small mammalian *in vivo* models. Zebrafish are vertebrate, jawed fish with a developed innate immune response that closely resembles that of mammals [25-27]. Key cell types for host-material immunological interaction, such as neutrophils and macrophages, have been identified and are well-characterized in the zebrafish [28]. However, unlike mammalian models, the zebrafish is conducive to real-time non-invasive imaging of the host-material interaction [29, 30]. The use of standard fluorescence microscopy with minimal specimen manipulation is possible due to the zebrafish's natural optical

transparency at early stages of development [31]. Using transgenic fluorescent reporter strains, cell populations of interest can be observed using fluorescence microscopy [30, 32]. After hatching from their chorion approximately 3 days post fertilization (dpf), the transparent embryos have easily distinguishable anatomical features, including a head with prominent eyes, main body cavity, trunk and yolk sac, which makes targeted implant placement feasible (Figure 1.1). However, at these early time points, zebrafish are only an average of 4 mm long, and typically no more than 300 µm thick in the trunk. These small sizes require the use of microscale techniques to perform biomaterial host interaction studies. Additionally, transgenic strains developed that lack pigment-producing cells, such as melanophores [33]. Compared to rodents, zebrafish have reduced maintenance requirements, with automated systems available to control water quality and perform feedings [34]. Additionally, zebrafish are a highly fecund species, with a single breeding event providing upwards of 100 viable embryos. [34].

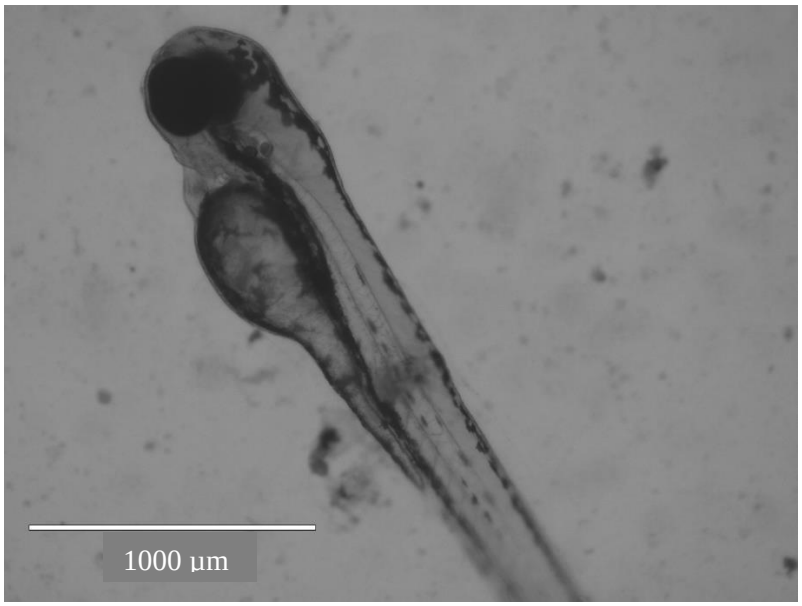

Figure 1.1: A 3 dpf zebrafish embryo. While the eyes are opaque, the remainder of the embryo retains transparency until reaching 20 dpf, at the juvenile stage.

The zebrafish has proven to be genetically tractable, with numerous transgenic strains available for examination of desired features, such as cell-specific labeling [35]. Despite these numerous advantages, there has been limited translation of this model into the biomaterials field, with only recent preliminary work performed. Preliminary studies were recently published on the acute inflammatory response to polymeric microparticles of varying sizes in zebrafish embryos [30, 32]. Additionally, initial work has been performed examining the adult zebrafish biomaterial host interaction [32]. However, these reports are very preliminary and to fully develop the zebrafish as a model for biomaterial research, a more robust approach to model development is necessary.

1.1 Thesis Scope and Specific Aims

The goal of this thesis was to develop a platform for the implantation and analysis of biomaterials in zebrafish embryos. This scope can be broken down into three specific aims.

Specific Aim 1: Establish a functional zebrafish colony at Queen's University, populated by both wild-type and transgenic strains.

Specific Aim 2: Establish experimental parameters for the injections of individual microparticles in zebrafish embryos, based on microparticle size and developmental stage of zebrafish.

Specific Aim 3: Develop a protocol for histological analysis of biomaterial host response in zebrafish embryos.

1.2 Approach

The first step in developing a biomaterial implant model in zebrafish embryos was procuring an initial set of breeding zebrafish adults, and establishing appropriate breeding protocols to begin a Queen's University zebrafish colony. After establishment of a colony that provided a consistent source of embryos, a strategy for implanting microparticles was developed. The microinjection technique was selected as it is frequently used to introduce molecules, cells, bacteria and other material into zebrafish embryos [32, 36, 37]. However, microinjection is generally used for injecting aqueous solutions and suspensions. Therefore, refinement of traditional microinjection techniques to enable the aspirating and injecting of solid microparticles was required.

Microinjections can be performed using either manual or pneumatic injectors. While pneumatic injectors provide precise control of the injection volume, microparticle settling within the needle tip can cause significant variations in the number of microparticles injected over time. With the goal of developing a robust and reproducible model, control over the number of microparticles injected in each embryo was considered to be an important criterion, as the number of microparticles implanted can modify the host response by increasing the surface area available for mediating cell-material interaction [5]. Conversely, manual microinjectors enable a user to implant a specific number of implants because microparticles are manually selected, aspirated, and injected. As examining the host-biomaterial model is the goal of this research, maintaining a consistent biomaterial volume and surface area within the embryo is paramount. As part of this development different sized microparticles were examined, ranging from 10 to 50 μm in diameter. In addition to the varying microparticle size, corresponding microneedle

adjustments were made. For each condition, implantation success, retention, and zebrafish viability was assessed.

While a major strength of the zebrafish model is its optical transparency, histology remains an essential tool for is still needed for analyzing tissue response to an implanted biomaterial in wild-type *in vivo* models. Early in model development, it became very apparent that histological analysis of zebrafish embryos would present a significant technical challenge due to the embryo size and delicate nature of the embryonic tissues. Consequently, histology protocols were established for analyzing the tissue of this model.

Chapter 2

Literature Review

2.1 Biomaterial Host Response in Mammals

Biomaterials have a broad array of applications, including tissue engineering scaffolds, drug delivery devices, or cell therapy treatments [6, 16, 38, 39]. While the intended application for a given material requires different testing conditions to ensure its use in a given area of the body is appropriate, such as drug release rates, or mechanical testing, the biomaterial host response must be evaluated for both established and novel materials, regardless of the application. The host-biomaterial interaction plays a critical role in the development of materials, because it often determines how well the host tissue will integrate with the biomaterial. In applications such as bio-monitoring or drug delivery there needs to be a high level of integration for the material to be effective, as the development of a fibrous capsule may interfere with the sensitivity of sensors or release rates of large molecules [40, 41]. This biomaterial host response can be compared to an aberrant wound healing response, in which the presence of a biomaterial interferes with normal progression of wound healing.

2.1.1 Wound Healing

Normal wound healing is traditionally organized into four overlapping stages: hemostasis, inflammation, granulation, and remodeling [42]. The first stage in the wound healing cascade is hemostasis, in which blood vessels that were damaged upon injury are plugged to prevent further blood loss [43]. Upon injury to a tissue, such as in surgical procedures, a cascade occurs in which platelets present in the blood stream bind together

at the wound site while secreting coagulation factors that promote the formation of a fibrin-rich blood clot [43, 44]. This fibrin-rich clot acts as both a barrier to prevent further blood loss, but also as a provisional matrix for leukocytes, fibroblasts and endothelial cells that participate in later stages of wound healing. Furthermore, the platelets within the clot secrete various factors, including transforming growth factor (TGF)-β1 and platelet derived growth factor (PDGF), that recruit cells from the surrounding tissue and vasculature to the wound site [42].

After hemostasis is restored, inflammation begins and neutrophils, monocytes, and macrophages begin invading the wound site [21]. During the acute inflammatory response, neutrophils rapidly accumulate within the wound to become the predominant cell population [10]. Neutrophils begin clearing the wound site of dead cells, debris and pathogens by phagocytosis [42]. After phagocytosing dead cells and debris, neutrophils will typically undergo apoptosis or migrate away from the wound site [42]. As the neutrophil population begins to decrease, monocytes reach the wound site and differentiate into classically activated macrophages [45]. Pro-inflammatory, or M1 type, macrophages secrete pro-inflammatory signals such as tumor necrosis factor alpha (TNF-α) and interferon gamma (IFN-γ) [46]. These pro-inflammatory macrophages persist at the wound site, enhancing phagocytosis and secretion of reactive oxygen species (ROS), such as hydrogen peroxide and superoxide anion [46]. As M1 macrophages continue secreting pro-inflammatory signals, they also begin secreting inflammation resolving factors such as TGF-β1 and vascular endothelial growth factor (VEGF) (Figure 2.1) [42]. As the inflammatory stimuli are cleared from the wound site, the predominant macrophage phenotype switches from a M1 phenotype to an M2, or pro-wound healing,

phenotype due to secretion of factors such as interleukin 4 and 13 (IL-4, IL-13) [47, 48]. The duration of the inflammatory phase will vary, depending on the severity of the wound, but generally begins to resolve within 2 – 4 days.

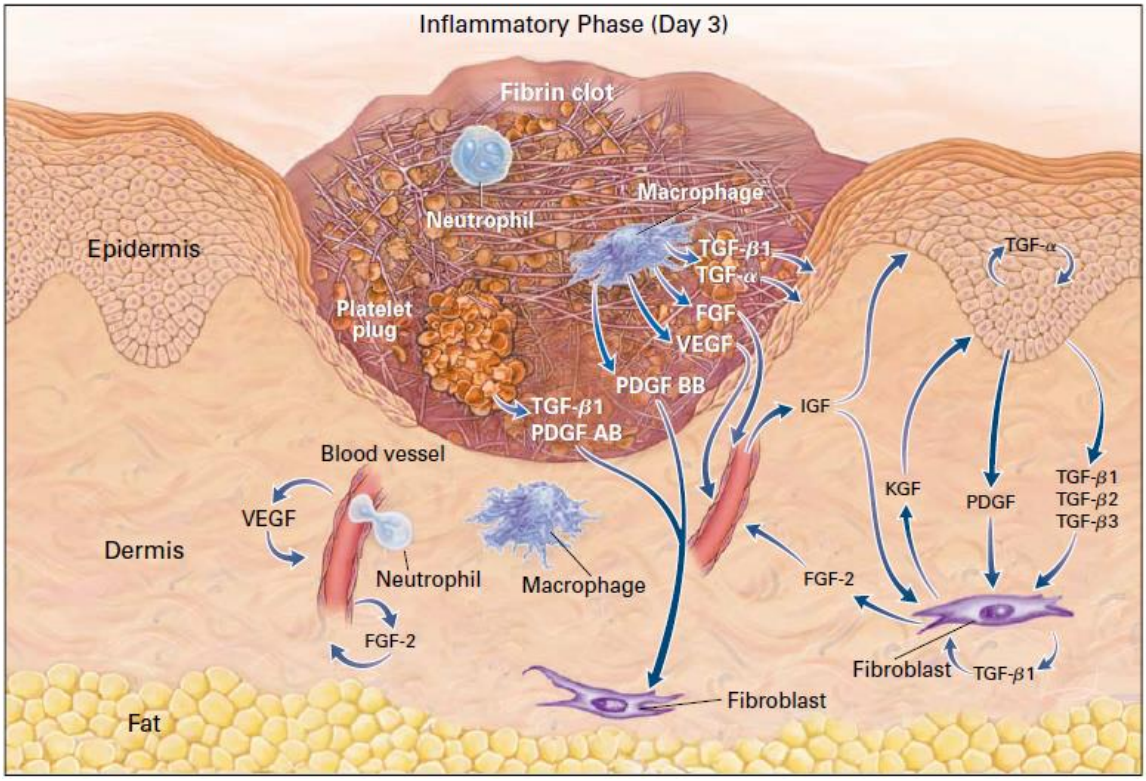

Figure 2.1: The typical inflammatory environment in a wound bed during early wound healing, with denoted cells types and secreted factors thought to be needed for the wound healing process. As platelets continue secreting factors to recruit cell populations, such as fibroblasts, M1 macrophages are secreting both pro-inflammatory and growth factors, such as TNF-α, and TGF-β. During this phase, early blood vessel formation is occurring due to secretion of VEGF. Additionally, fibroblasts are recruited with secreted FGF, fibroblast growth factor. Reproduced with permission from Singer and Clark, 1999 [42], Copyright Massachusetts Medical Society.

As inflammation begins to resolve, M2 macrophages cease secreting macrophage recruitment factors in large quantities and begin to secrete factors that promote the subsequent stage of wound healing [42]. These factors include VEGF, TGF-α, TGF-β1, and PDGF, which recruit fibroblasts, and endothelial cells from the surrounding tissue [42]. The transition from the inflammatory phase to granulation (or tissue formation) is

marked by a reduction in macrophages within the wound, and the infiltration of fibroblasts that begin replacing the fibrin-rich provisional matrix with a collagen-rich granulation tissue [42].

During granulation, macrophages continue to provide a source of growth factors with the purpose of stimulating tissue formation and vascularization of the wound bed [42]. In response to secreted growth factors, such as fibroblast growth factor (FGF), and TGF-β1, fibroblasts begin secreting a collagen-rich matrix or granulation tissue. Additionally, fibroblasts begin stimulating the growth of surrounding cell populations, such as keratinocytes in a skin wound, by secreting keratinocyte growth factor (KGF) [42]. Endothelial cells sprout from surrounding blood vessels in a process called angiogenesis, in response to the increased cellular burden within the wound and angiogenic growth factors secreted by macrophages, including VEGF, PDGF, and FGF-2 [4, 38]. These new blood vessels form an immature vascular network in the wound bed and provide the required nutrients to support the high metabolic demand of wound healing [49]. The granulation tissue deposited by fibroblasts act as a matrix, in which cells can grow, restoring the tissue to a non-injured state (Figure 2.2) [42]. It is during this phase that re-epithelization occurs, which is stimulated by secreted growth factors such as KGF, among others [48]. The hyperproliferating keratinocytes at the wound edge begin to migrate from the outer edges of the wound bed inward, restoring the epithelial integrity of the skin [16]. The leading edge of the migrating keratinocytes bisects the fibrin clot from the underlying granulation tissue, and the fibrin clot is sloughed off as the eschar (or scab) in external wounds, or degraded and phagocytosed in internal wounds [27, 50]. It is during this phase that macrophages present at the wound site begin to decrease, and

fibroblasts begin secreting growth factors and enzymes meant to degrade the provisionary clot on the surface of the wound [42, 50]. Towards the end of the proliferation stage, fibroblasts and myofibroblasts begin remodeling the tissue.

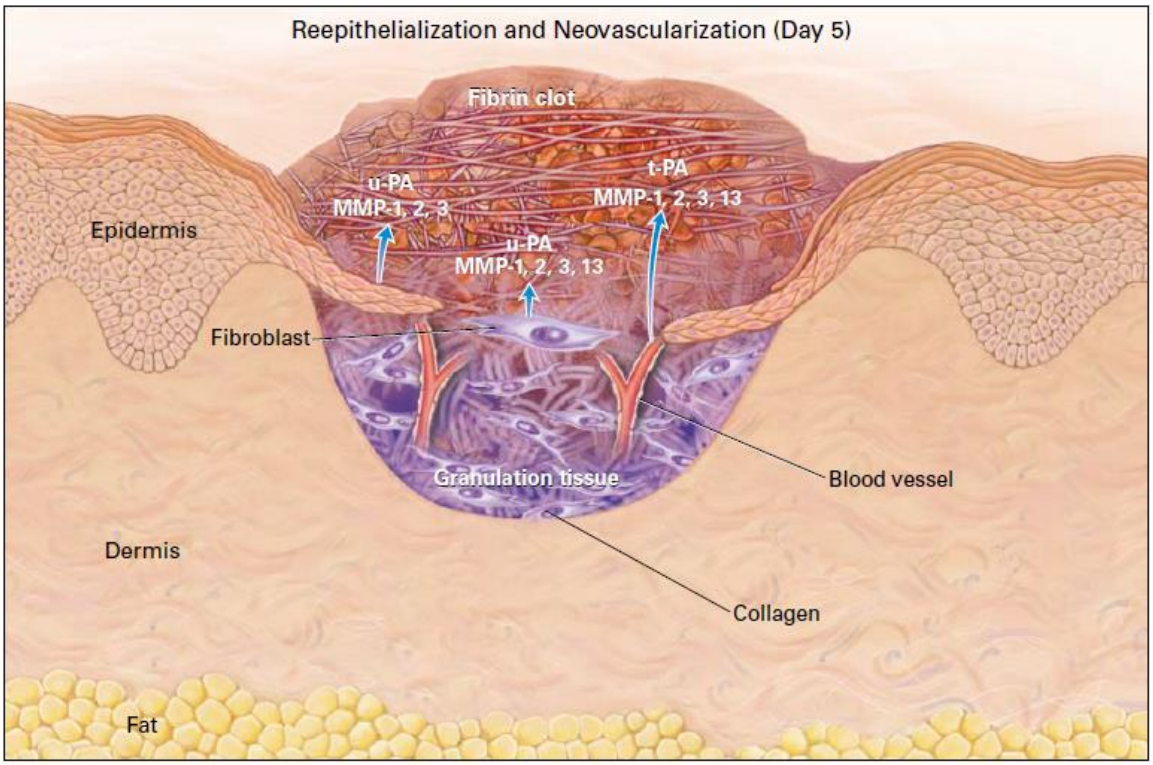

Figure 2.2: A schematic representation of the granulation phase of wound healing. Fibroblasts deposit a collage-rich matrix and secrete various factors, such as metalloproteinases (MMP) to promote the degradation of the fibrin clot. Endothelial cells migrating into the wound bed to establish an immature vascular network to support tissue repair. Reprinted with permission from Singer and Clark, 1999 [42], Copyright Massachusetts Medical Society.

Remodeling can take weeks to months to complete [42]. As the granulation tissue and re-epithelization expands to cover the wound site, fibroblasts begin differentiating into myofibroblasts in response to TGF-β and other factors [42]. Myofibroblasts are a contractile cell population that contracts and reorganize the granulation tissue, while continuing to secreting extracellular matrix (ECM) components such as collagen [51]. Overtime, the cell density within the granulation tissue decreases as the matrix is remodeled, and the immature vascular network established during granulation regresses.

The resulting tissue is a relatively acellular, avascular scar tissue [42]. The contractile forces on the wound site reduce the granulation tissue size by as much as 40%, and increases the strength of the new tissue [51]. While wound healing results in tissue repair, the complete structure and function of the original, native tissue is rarely regenerated [27, 52].

2.1.2 Foreign Body Reaction

Chronic inflammation in humans occurs when the inflammatory phase persists. This extension can be caused by several factors, including pre-existing conditions hindering the immune response, such as diabetes, or the presence of a foreign body, such as a biomaterial, within the tissue [21]. In the instance of a foreign body, the host will exhibit the foreign body reaction (FBR) (Figure 2.3). Upon implantation, biomaterial surfaces become immediately covered in a layer of proteins that present epitopes that signal damage to investigating neutrophils and macrophages, as well as providing integrin binding sites for adhesion [53, 54]. As neutrophils begin clearing the implant site of damaged tissue, macrophages reach the surface of the biomaterial and attempt to phagocytose the implant. However, macrophages are typically unable to directly phagocytose anything larger than 10 μm, and most implants are larger than this [55]. As inflammation persists, macrophages continue secretion of ROS such as hydrogen peroxide or superoxide anion, to break down the biomaterial [10]. In addition to breaking down the biomaterial, the secreted ROS also damage the surrounding tissue and perpetuate inflammatory responses [10, 13]. If the biomaterial is unable to be degraded and removed, macrophages will undergo frustrated phagocytosis and fusion to form multinucleated, foreign body giant cells (FBGC) [56]. In addition to continuing to secrete

a range of degradative enzymes and reactive oxygen species at the material interface, adherent macrophages and FBGC also release signaling factors to recruit fibroblasts to deposit a fibrous capsule around the implant [17].

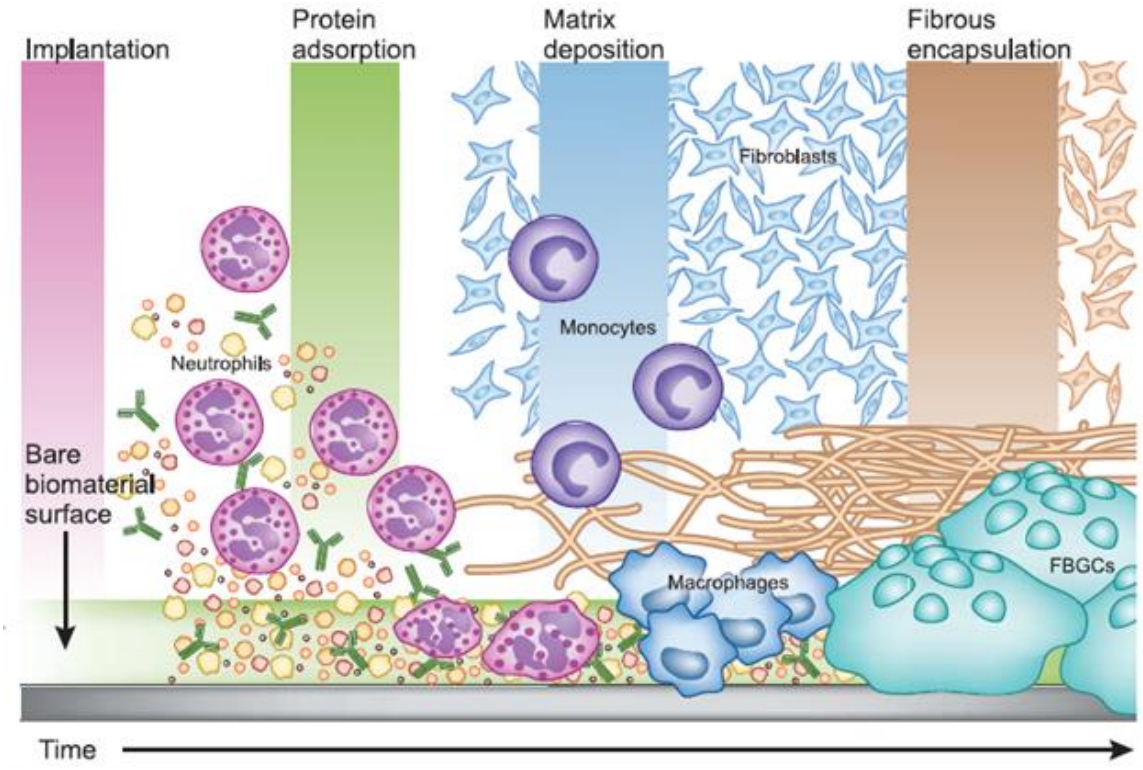

Figure 2.3: The foreign body reaction to an implanted biomaterial. The FBR is initiated by protein adsorption on the material surface, followed by the interrogation of these proteins by integrins on the surface of neutrophils and macrophages. Once inflammation has begun macrophages attempt to degrade the surface of the biomaterial. When the macrophages are unable to remove the biomaterial, frustrated phagocytosis occurs and macrophages begin fusing into foreign body giant cells (FBGCs). Ultimately, as macrophage and FBGCs continue secreting degrading enzymes, fibroblasts secrete an acellular, avascular matrix around the implant. Reprinted with permission from Grainger, 2013 [54].

This fibrous capsule has low vascularization and acts as a barrier, preventing interaction of the biomaterial with the host. Furthermore, the thickness of the resulting fibrous capsule can vary depending on several factors, including the implant size, chemistry, and surface topography [14, 17, 20, 57-59]. For instance, microfibers of poly(l-lactic acid) implanted subcutaneously for 5 weeks in rats developed a significantly thicker capsule ($p < 0.05$) than microfibers of the same diameter made of poly(urethane) [58]. Furthermore,

increasing fiber diameter was demonstrated to increase the resulting fibrous capsule thickness across all polymer types [58, 59].

In vivo characterization of FBR is done by examining the surfaces of implanted biomaterials, typically using histological or immunohistochemical techniques [10, 11]. Furthermore, degradation products and chemical species can be detected through various techniques, such as spectrophotometry and ELISA assays) of the explanted material [9, 60]. Staining can be done on target molecules to examine general cellular infiltration of key cell populations such as neutrophils (CD11b), macrophages (CD68), endothelial cells (CD31 and CD34), and myofibroblasts (smooth muscle actin), in a chronic wound [61-64]. Additionally, angiogenesis can be monitored indirectly via endothelial cell growth and vessel formation [63]. Furthermore, tissue staining can be performed for matrix proteins, such as collagen, to quantify fibrous capsule thickness. These stains include hematoxylin and eosin (H&E), and Masson's trichrome [65, 66]. These traditional methods only offer snapshots of a complex and dynamic process, which can cause problems for identifying and evaluating the full process of the FBR. This type of end-point analysis may result in key events being missed within the FBR due to pre-determined observation time-points. Conversely, real-time or time-lapse imaging enables the observation of the biological process in its entirety, and avoids the risk of missing a key observation or event that falls outside of a pre-selected end-point.

Imaging techniques have been developed that allow for real time imaging of the chronic wounds in rodents, such as window models and intravital imaging (Figure 2.4) [22]. However, these real- time models do have limitations. Window chamber models can

interfere with the host response due to the surgical requirements for producing the window chamber itself [19].

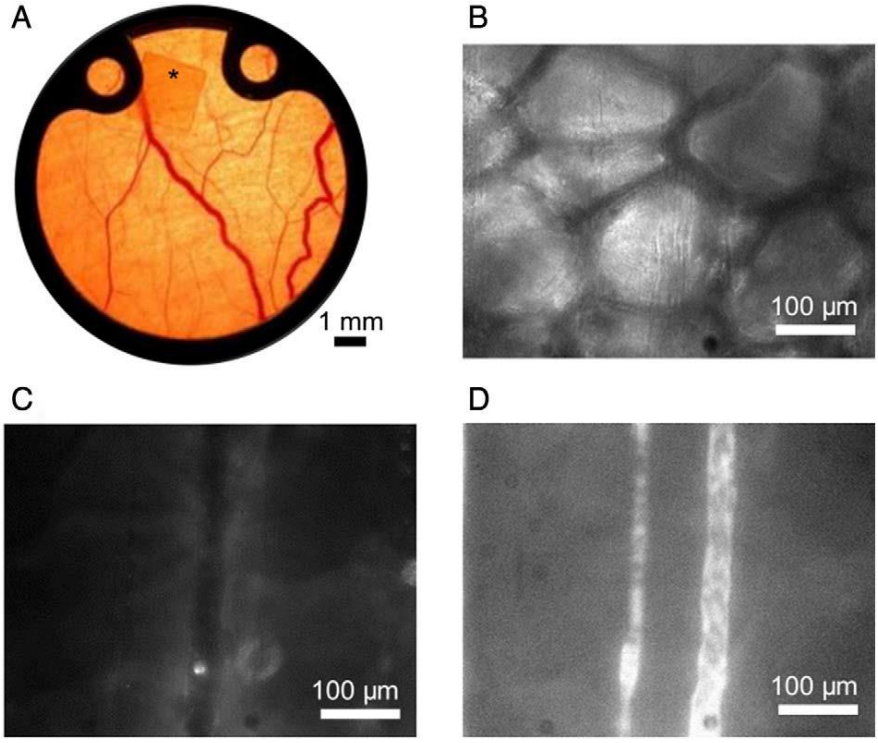

Figure 2.4: A) Photograph of dorsal skinfold chamber of Syrian golden hamsters, containing striated muscle and skin and allowing for repeated analysis of the microcirculation in an awaken hamster for two weeks. (B, C, D) Representative intravital fluorescence microscopy image of the microcirculation under an implant 15 days after implantation at 20x magnification. Reprinted with permission from Damestani *et al*., 2016 [22].

By causing tissue damage around the implant site, the host response can be modified, making material specific responses difficult to determine [19]. Additionally, intravital imaging does not allow the tracking of cells in situ. However, alterative animal models do exist that can be imaged using fluorescent microscopy without such limitations. One such model is the zebrafish, which is the focus of this thesis.

2.2 Zebrafish as an Animal Model

Danio rerio, or zebrafish have been used as a comparative model of embryogenesis for over 100 years, due to their external fertilization and transparent appearance of the

chorion and embryo during early development [26]. These features make identification of developing structures vastly simplified compared to mammalian models. Their external fertilization also made genetic manipulation and development of new zebrafish strains possible, providing a powerful tool for developmental biologists. In the mid-1970's, their genetic tractability was first demonstrated with the development of new reporter strains of zebrafish that were used to identify specific cell types, such as neutrophils and macrophages [35, 67]. Since this time, zebrafish have been explored as a model for a wide range of scientific fields, from social behavior to infectious diseases [68, 69].

2.2.1 Zebrafish Biology and Development

Zebrafish are class of teleost, or jawed, fish [70]. As teleosts and humans separated evolutionarily from one another roughly 450 million years ago, there are significant differences in the developmental cycle, size and morphology between zebrafish and mammals [70]. Zebrafish have four distinct stages of development, beginning with the embryo, and proceeding to larvae, juvenile, and finally adult [31, 71]. Eggs are laid in clutches of upwards of 100 per female, and are fertilized *ex vivo*. Fertilized eggs have a shell-like chorion that surrounds the embryo, which consists of a yolk sac and cluster of developing cells (Figure 2.5) [31]. Eggs are spherical, and are typically 0.5 - 1 mm in diameter [31]. Embryos hatch from their chorions two to three days post fertilization (dpf) [31]. At this stage, embryos are 2 to 3 mm in length, and have a functional cardiovascular system [31]. The innate branch of the immune system, including neutrophils and macrophages, is also functional by 3 dpf [31]. The larval stage of zebrafish develop begins at 5 dpf, when embryos are roughly 5 mm in length, and require

an external food source as the yolk sac is depleted [72]. At this age, pigmentation in wild-type zebrafish begins to develop, as well as scales [31, 73].

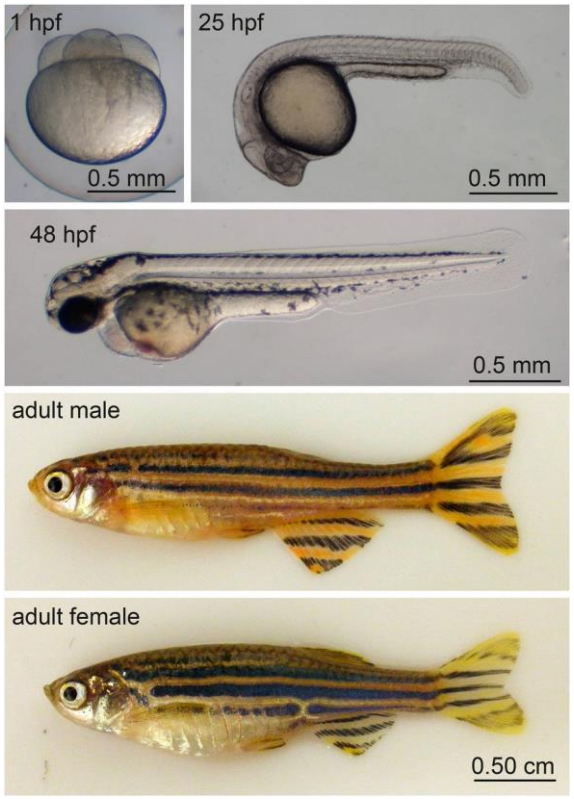

Figure 2.5: Developmental stages of the zebrafish development. 1 hour post fertilization (hpf), the egg is fertilized and is classified as a blastula. By 48 hpf, the embryo has a defined head, trunk and yolk sac. The zebrafish reaches adulthood at 3 months post fertilization. At this stage, zebrafish are no longer transparent and have a fully developed scale system. Reprinted with permission from Holtzman *et al*., 2016 [74].

By 15 dpf, zebrafish larvae are now fully reliant on external food sources, and their gastro intestinal tract has fully developed to replace the yolk sac [70]. Scales have developed, and pigmentation has reduced transparency. At 30 dpf, the zebrafish are considered juveniles, with fully functional organ systems, colored scales and are approximately 10 mm long [71]. The adaptive immune system begins developing at this time and is fully functional by 6 weeks post fertilization[69]. Zebrafish enter adulthood and are sexually mature at 90 dpf, at which point females begin continuously producing eggs, and can produce clutches once a week [34]. Adult zebrafish have a final length of

roughly 25 mm, and remain in an ideal breeding stage until 18 months of age, when females begin decreasing egg production [70]. In captivity, zebrafish have an average life span of 3.5 years [70].

Identification of genetic mutations and direct genetic manipulation of the wild-type zebrafish have led to the generation of a rich library of mutant, knock-out and reporter zebrafish strains [75]. An extremely useful transgenic model is the Casper strain, which lacks both melanocytes, which provide pigmentation, and reflective iridophores, responsible for the reflective properties of scales [33]. The loss of melanocytes is attributed to mutation in the *mitfa* gene, and the loss of reflective iridophores is attributed to a mutation in the *tra* gene [33, 76]. The lack of pigmentation throughout the life-span of the zebrafish allows the long-term observation of development of sexual organs and other, late stage phenomena [33]. It is frequently used as a background strain for transgenic reporter strains, that express fluorescent proteins, such as green fluorescent protein (GFP) or mCherry, under a specific promoter. This enables tracking of specific cell populations, including neutrophils and macrophages [35, 77], or the expression pattern of specific proteins, such as liver-type fatty acid binding protein [78]. There is a wide array of knockouts and reporter lines available to allow researchers to target specific interactions within the zebrafish, and provide more tools than other common *in vivo* models.

2.2.2 The Zebrafish Immune System

The zebrafish innate immune system contains many of the key cell populations associated with the host-biomaterial interaction in humans, including monocytes, macrophages, and neutrophils [79]. Furthermore, these cell types have been identified as having similar

functions to their mammalian counterparts [77]. However, there are differences in the organization and development of the zebrafish and mammalian immune systems [79]. For example, the zebrafish lymphatic system does not include lymph nodes, although the lymphatic vessels and spleen, a secondary lymphatic organ, are present [79].

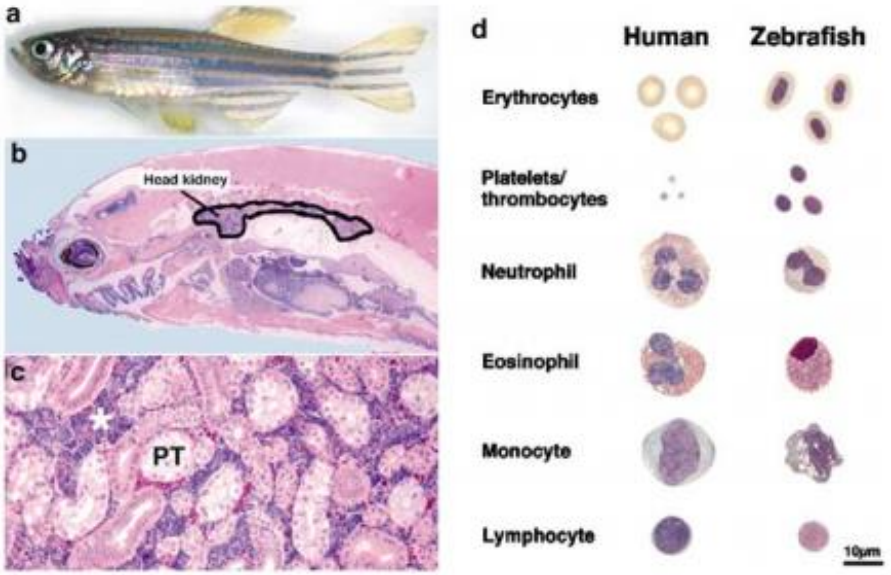

Figure 2.6: Hematopoiesis in adult zebrafish kidney and morphological comparison of human and zebrafish blood cells. a) Adult zebrafish, male (2.5cm in length). b) Para-sagittal section of an adult zebrafish stained with hematoxylin and eosin, with outline of head kidney in black. c) Higher magnification view of head kidney showing mesonephric tubules (PT) surrounded by small blue- and red- stained hematopoietic cells (white asterisk). d) Comparison of human and zebrafish mature peripheral blood cells stained with Wright Giemsa. Reprinted with permission from Davidson and Zon, 2004 [79].

Additionally, the site of hematopoiesis differs between zebrafish and mammals. The hematopoietic stem cell population, which gives rise to neutrophils, monocytes and all other blood cells, resides in the bone marrow in mammalian species [80]. Conversely in zebrafish, the hematopoiesis occurs in the "head kidneys", a structure located dorsally to the gastro-intestinal tract (Figure 2.6) [79].

A critical feature of the zebrafish immune system, given the scope of this thesis, is the temporal delay between the development of the innate and adaptive branches of the

immune system. The zebrafish embryo begins expressing functional innate immune cells, including monocytes, macrophages and neutrophils, by 2 days post fertilization [77]. Whereas the adaptive immune system, characterized by the presence of T and B lymphocytes, does not become fully functional until 4-6 weeks post fertilization [36]. This large temporal delay in the development of the adaptive immune systems provides a window in which the innate immune responses can be examined in isolation, without requiring the genetic manipulation of the wildtype fish that can introduce unintended off-target effects. However, as crosstalk between adaptive and innate immune systems are known to effect inflammatory responses, including host-biomaterial interactions, the absence of an adaptive arm of the immune system is an important consideration when using zebrafish as a comparative model [11]. Despite these differences, zebrafish are widely used to study innate and adaptive immune responses, hematopoiesis and hematopoietic stem cell transplants [29, 65, 81]

2.2.3 Zebrafish as a Model of Wound Healing and Microbial Infection

Zebrafish have been used extensively as a disease progression model due to analogous diseases shared with humans [36, 66, 82, 83]. Most notably is the similar progression of *mycobacterium marinum* in zebrafish and *mycobacterium tuberculosis* in humans. Both diseases target innate immune cells, specifically macrophages, as their primary replication site [29, 69]. Once infection has occurred, both *M. marinum* and *M. tuberculosis* begin rapidly replicating and causing massive damage to surrounding tissues [69, 82]. In zebrafish, this can rapidly lead to death, and this response is enhanced if infection at the embryonic stage [29]. This progression is similar to humans, in which M. tuberculosis is phagocytosed by alveolar macrophages, but continues to proliferate

intracellularly [84]. Furthermore, in both diseases, the host produces granulomas to isolate the infected macrophages [29, 85].

In addition to insights gained from bacterial replication and disease progression, zebrafish bacteria can be treated with novel drugs for their human counterparts [82]. Due to the transparent nature of zebrafish, this model allows direct monitoring of bacterial infection and drug efficacy using microscopy in real-time (Figure 2.7) [82].

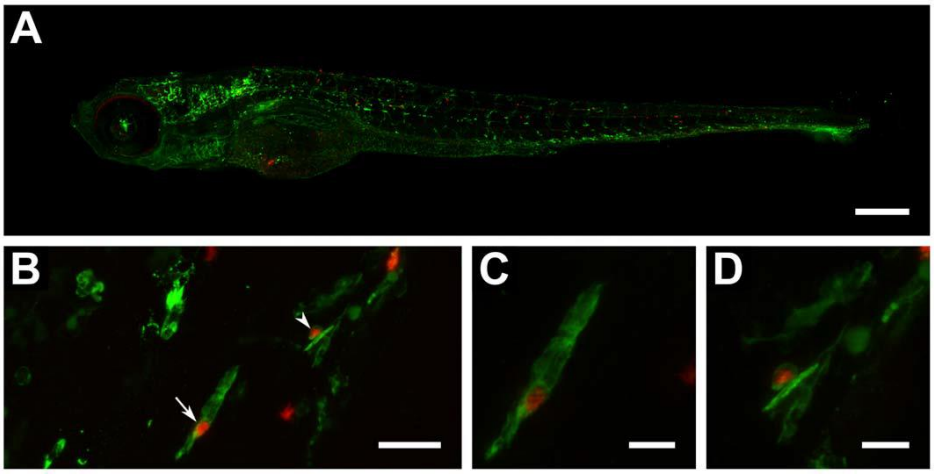

Figure 2.7: A) A confocal z-stack of a 6-day old whole larva (fli1-eGFP with gfp-labelled vasculature) showing spread of bacteria (red) throughout the body. Scale bar is 250 µm. B) Confocal z-stack of red-fluorescent bacteria co-localizing with green fluorescent leukocytes detected by L-plastin immunostaining. Scale bar is 25 µm. C) Digital zoom of bacteria-containing leukocyte depicted in B by straight arrow. Scale bar is 10 µm. D) Digital zoom of bacteria-containing leukocyte depicted in B by arrowhead. Scale bar is 10 µm. Reprinted with permission from Carvalho *et al*., 2011 [82].

The high fecundity of zebrafish allows trials to be carried out with high-throughput testing [82]. The possibility of high-throughput testing has led to the development of several micro- and milli-scale devices that enable rapid capture, infection, and treatment of disease, with rates of over 1000 animals every hour (Figure 2.8) [82]. By developing these high throughput testing platforms for zebrafish, researchers will be able to generate trials that will mimic population wide responses, or perform parallel testing multiple drug candidates or potential toxins [69, 82, 86-88]. Furthermore, these trials will not be limited

to end-point analysis, as developing technology enables real time progression of diseases and infection using fluorescence tracking of individual cell populations [82]. The ability to perform high-throughput, real time analysis will further increase the power of each trial.

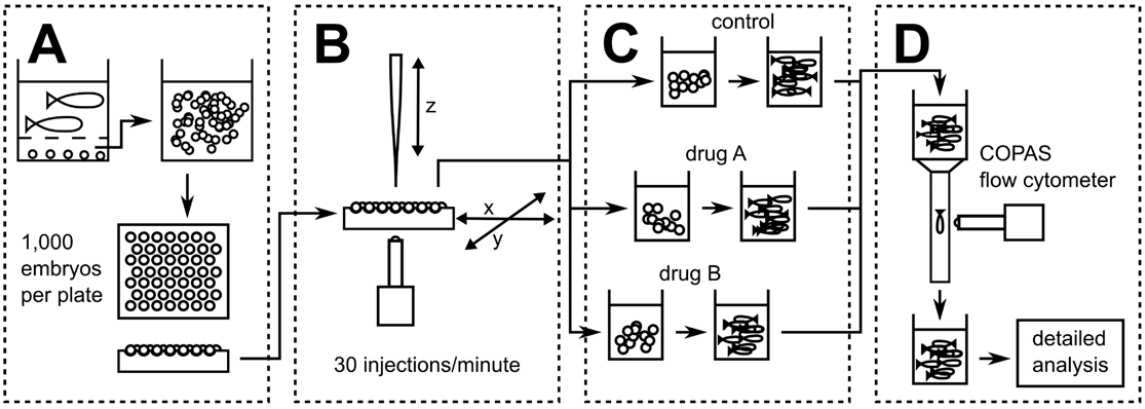

Figure 2.8: The workflow of high-throughput infection of zebrafish embryos and subsequent drug testing. a) Fertilized eggs are harvested, washed and distributed on injection plate. b) Inoculum is injected in early stage embryos (up to the 1024 cell stage). c) Injected embryos are dispensed into appropriate containers and drug screens take place between 3 and 6 dpi. D) Groups of treated and untreated embryos are separately screened using complex object parametric analysis during (when appropriate) and after drug exposure. Reprinted with permission from Carvalho *et al*., 2011 [82].

2.3 Zebrafish as a Model of Biomaterial Host Responses

Until 2017, zebrafish had received very little interest as an animal model in the biomaterials field. However, two recent publications have begun examining the zebrafish as a model for host-biomaterial interaction at both the adult and embryo stage [30, 32]. In adult zebrafish, hallmarks of a chronic inflammatory response to an implanted poly(ethylene) suture has been observed over the course of 21 days [32]. The host response was characterized using histological analysis of the implant sites using Masson's trichrome to determine collagen capsule thickness (Figure 2.9g-k) [32]. Additionally, the accumulation of leukocytes, identified by the pan-leukocyte marker L-

plastin, at the implant site was also examined as a measure of the inflammatory response to the suture (Figure 2.9l-p) [25, 32].

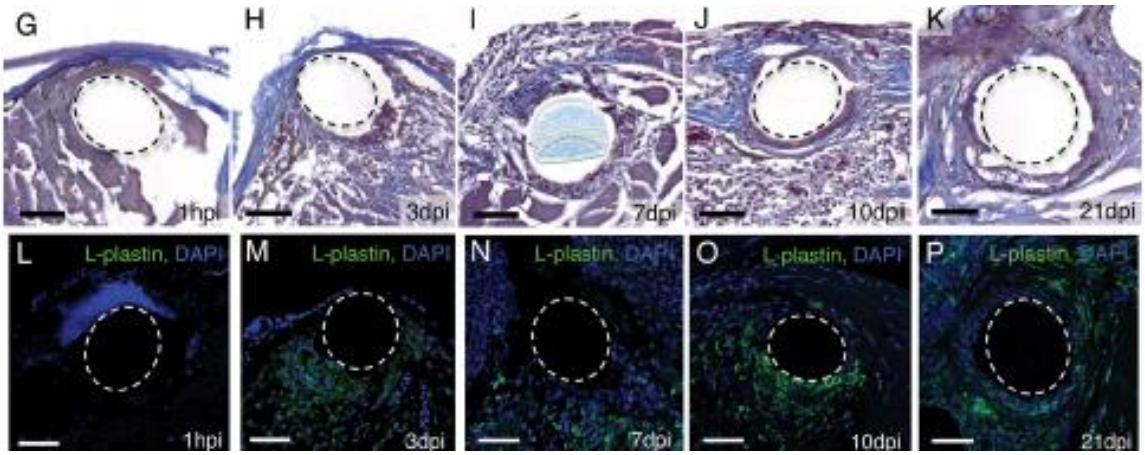

Figure 2.9: Suture implantation in adult zebrafish, collagen deposition and innate immune cell tracking over 21 dpf. (G-K) Masson's trichrome staining to examine collagen deposition around implant (circled in black dotted line) over 21 days. (L-P) L-plastin and a nuclear DAPI staining to examine presence of innate immune cells over 21 days post implantation with implant within the circled area with a white dotted line. Scale bars are 30 µm. Reprinted with permission from Witherel *et al*., 2017 [32], copyright American Chemical Society.

An increased presence of L-plastin-positive cells, compared to sham controls, was observed at the surface of the implant for the duration of the 21 day study, indicating the suture elicited a chronic inflammatory response [14, 17, 89]. Furthermore, collagen deposition occurred over the course of 21 days, and increased in thickness over this time period [32]. The sustained leukocyte presence and fibrous capsule deposition at the suture surface suggests that the adult zebrafish exhibits a chronic inflammatory response like the foreign body reaction observed in mammals [10].

Examination of the embryonic immune response has also yielded promising results for modeling an acute host-biomaterial interaction, as seen in Figure 2.10 [32]. However, the results from the two studies reporting on the acute inflammatory response in embryos are somewhat inconsistent [32].

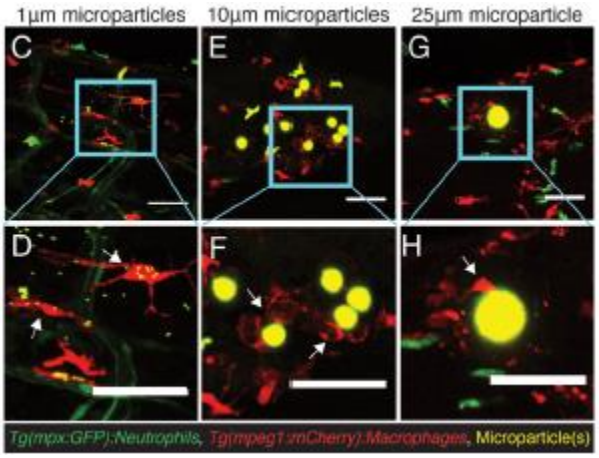

Figure 2.10: Implanted microparticles at 3 days post injection (dpi) at various sizes. The transgenic strains used were *Tg(mpx: GFP;mpeg1: mCherry)* the microparticles are poly(styrene) with yellow fluorescent labelling. c, d) Representative images from movies of a larval zebrafish implanted with 1 µm polystyrene microparticles. Note that the representative image from the 1 µm microparticle group was taken with a triple transgenic fish, *Tg(f li1: GFP, mpx: GFP, mpeg1: mCherry),* in which macrophages are labeled red and both neutrophils and endothelial cells are labeled green. e, f) Larval zebrafish implanted with 10 µm polystyrene microparticles. g, h) Larval zebrafish implanted with a single 25 µm polystyrene microparticle. All images are from zebrafish 3 dpi, represented as a z-stack projection of maximum intensity, and scale bars are 50 µm. Reprinted with permission from Witherel *et al*., 2017 [32], copyright American Chemical Society.

In one study, injections were performed with 1, 10 and 25 µm poly(styrene) (PS) microparticles [32]. The number of microparticles injection per embryo variable for both 1 and 10 µm microparticles, ranging from 40 – 90 microparticles/embryo and 5 – 12 microparticles/embryo, respectively. A single microparticle implant was injected at the 25 µm size. Manual cell counts performed post injection determined macrophages and neutrophils accumulation around the implant site increased upon implantation by 1 dpi, but returned to baseline after 5 dpi [32].. Furthermore, in both the 1 and 10 µm implant sizes, an average of 36.5% and 28.1% of microparticles were phagocytosed, respectively [32].

In the study performed by Zhang *et al*., injections were performed with 10 and 15 µm PS microparticles, with some embryos receiving up to eight microparticles in a single

injection, however statistics were not reported for this variance [30]. While it was observed that neutrophils and macrophages interrogated the surface of the material within 1 dpi, both cell populations returned to baseline at 4 dpi, with a marked decrease occurring at 2 dpi [30]. Furthermore, Zhang *et al*. used a fixed 100 µm area around the injected microparticle, determined by initial injections, to perform cell counts [30]. However, Zhang *et al*. did not report on microparticle migration and phagocytosis of 10 µm microparticles, as had been observed by Witherel *et al.* [30, 32]. Furthermore, the number of microparticles implanted per embryo was also reported as variable but exact ranges were not provided, making a direct comparison between the two studies challenging. These differences in methodology could explain the differences observed in the macrophage and neutrophil presence over a period of one week. In both studies, the early resolution in inflammation to an implant is inconsistent with the persistent presence of macrophages observed mammalian responses [9]. However, could be explained by a lack of T and B cells [11, 90]. Indeed, the persistence of L-plastin labelled cells and the deposition of a collagen capsule in adult zebrafish (Figure 2.9) suggests that adult zebrafish are more appropriate for studying chronic inflammation and fibrosis [32].

Witherel *et al*. also demonstrated conservation of IL10's anti-inflammatory nature within the zebrafish model [32, 91]. PS microparticles with adsorbed zebrafish IL10 were injected into the trunks of zebrafish embryos produced a significant decrease of leukocyte numbers at the surface of the microparticle compared to blank microparticle injections [32]. The conservation of molecular function and demonstrated response to IL10 delivery further highlights the use of zebrafish as an animal model.

2.4 Selection of Model Biomaterials

2.4.1 Model Constraints

Several constraints were considered when selecting appropriate biomaterials for this preliminary work in developing a zebrafish embryo biomaterial implant model. The first constraint we considered was what polymer chemistries would provide a simple and reproducible material for this proof-of-principle work. Non-biodegradable materials offered a simplified host-biomaterial interaction as the material properties would remain relatively constant and no degradation products would be produced over the duration of the study [18, 89]. Degradation products can alter the pH of the surrounding environment, which has been known to effect the immune response [18]. By selecting non-degradable materials, the observed response could be attributed to the biomaterial itself. Another constraint was implant volume, which was a critical constraint due to minute size of zebrafish embryos. An initial microparticle diameter range of 10 – 100 μm was selected. The upper limit of 100 μm was identified, because implants of this size would occupy 40% of the zebrafish trunk width. The lower limit of 10 μm was selected to avoid phagocytosis of the implants, which has been observed in zebrafish for microparticles under 10 μm in diameter [32]. Finally, to take advantage of the inherent transparency of zebrafish embryos, microparticles should be fluorescently labeled to assist in implant identification, as well as commercially available to allow the thesis to focus on the implant model, rather than material generation, characterization, and purification.

2.4.2 Biomaterial Selection

Based on these constraints, two model polymers were chosen: poly(styrene) and poly(ethylene). Both polymers are non-degradable, can be tagged with fluorescent labels,

and are readily available through commercial suppliers [17, 92]. Importantly, both polymers have been studied extensively in mammalian models of host-biomaterial interactions, and exhibit a chronic inflammatory response resulting in FBR [13, 17, 92-94].

As a biomaterial, poly(styrene) has been examined for its use as a microparticle, drug delivery vehicle and is the most prevalent cell culture substrate [17, 32]. Furthermore, it has a well characterized and reproducible biomaterial host response that supports the use of the material as a testing material for new models [30]. Poly(ethylene) is one of the most common polymers used globally [95, 96]. It has been used in several applications for biomedical devices, such as a vascular replacement, or drug delivery device [97, 98]. By using these well-characterized materials, the host response between species can be compared to identify similarities and differences in the innate immune responses to implanted materials. This will help validate zebrafish as a model, but will also assist in exposing its limitations by highlighting key differences between the host response of zebrafish and other models to these well-characterized biomaterials.

2.4.3 Fluorescent label selection for microparticle

The proposed zebrafish model aimed to take advantage of fluorescence imaging and transgenic zebrafish strains to study material host responses in whole organisms. Consequently, the implanted materials required a fluorescent label to enable their identification using fluorescence microscopy. In order to easily distinguish the implanted material from cells, it is critical that the fluorophore used to label the material has a peak emission wavelength that is distinct from the fluorescent proteins used to label cell populations of interest in the transgenic zebrafish strains.

The transgenics selected for this work contain eGFP labeled macrophages and neutrophils. EGFP is a 27 kDa protein that has an excitation wavelength of 488 nm [99]. Upon absorption of a photon at these wavelengths, the protein emits an excited photon at 509 nm [99]. To prevent fluorescent confounding, two common fluorescent labels were chosen that do not emit in this range: 4',6-diamidino-2-phenylindole (DAPI) and Texas Red, which have peak emissions of 461 nm and 615 nm, respectively [100, 101]. The differences in emission spectra between these three fluorophores will allow easy differentiation upon examination of injected embryos.

2.5 Summary

While inflammation is a natural part of the healing process, chronic inflammation and FBR are undesirable outcomes for host-material interactions that can impact the performance of the material and/or device, or the surrounding tissues [10]. The FBR is commonly studied using small animal models, which limits the examination to end-point techniques, such as histological or immunohistochemical (IHC) staining [19, 22]. These end-point analyses require pre-determined time points, which can result in missing key transitions during inflammation. Zebrafish can offer the ability for real time, noninvasive investigation of the FBR and how neutrophils, macrophages, and other cell populations interact with the biomaterial implants [17, 32]. Preliminary work examining the zebrafish as a potential model has yielded promising results, but a more robust platform must be developed to establish zebrafish as an accepted model of biomaterial host responses.

Although beyond the scope of this thesis, a future goal for this biomaterial implant model is to provide a quantitative analysis of the inflammatory response to the implanted material. To achieve a robust and reproducible model, the effect of microparticle volume,

surface area to volume ratio, and number of implanted microparticles must be considered. These factors have demonstrated effects on the final fibrous capsule formation and play an important role in the FBR [58, 59, 102].

Chapter 3

Materials and Methods

3.1 Ethics Statement

All experiments were approved by the Queen's University Animal Care Committee (Protocol 2015-1523) and followed the Canadian Council on Animal Care guidelines.

3.2 Zebrafish Husbandry

3.2.1 Colony Housing and Maintenance

The Fitzpatrick zebrafish colony was housed on a semi-closed, re-circulating system with an automated buffering/monitoring system and biofilter (ZebTEC Active Blue Stand Alone System, Tecniplast, Italy). The automated buffering system maintained the water quality at the following set points: conductivity of 500 µS/cm, temperature of 28° C and pH of 7.0. The conductivity and pH were controlled by automatic dosing pumps that added a synthetic salt solution (30 g/L, Instant Ocean® Sea Salt, Virginia, USA) and sodium bicarbonate (30 g/L, Fisher Scientific, S233-3, Fisher Scientific, Ontario, Canada) as needed. Ammonia levels were controlled by a biofilter containing nitrifying bacteria. In addition, ammonia readings were taken daily using an API Ammonia Test Kit (Catalog No. API LR8600, Mars Fishcare, New York, USA) to ensure ammonia levels were maintained below 2 ppm. Nitrite and nitrate levels were measured once a week using an API nitrite and nitrate testing kit (Catalog No. API item #34, Mars Fishcare).

Static quarantine tanks were used to house adult fish brought into the colony from outside of Queen's University to avoid the potential introduction of pathogens into the main colony housed on the recirculating system. Quarantine water ammonia and pH levels

were measured daily, as described in 3.2.2. As needed, water quality was maintained by performing water exchanges, in which 3.5 L of quarantine tank water was removed and replaced with 3.5 L of water taken off the Tecniplast system (referred to as "system water"). Adult quarantine fish were fed as described above. Quarantine adults were observed for 2 weeks for signs of disease or infection, prior to breeding.

3.2.2 Adult Breeding Stock

Tübingen (TU) wildtype zebrafish were procured from the Toronto SickKids Hospital (Ciruna colony, Ontario, Canada). Two transgenic strains, *Tg(mpx: eGFP)* and *Tg(mpeg: eGFP)* with a Casper background, were procured from the Zebrafish Core Facility at the University of Dalhousie (Dalhousie colony, Nova Scotia, Canada). Adults were maintained in quarantine, as described in 3.2.1, until a sufficient population of in-house bred transgenics were obtained, after which quarantined adults were euthanized as described in 3.2.4.

Adult breeding stocks on the Tecniplast recirculating system were housed at a density of 15-20 fish per 3.5 L aquarium, or 20-30 fish per 8 L tank. Quarantined adults housed in the 10 gallon (37.8 L) static tanks were maintained at a lower density of 12-25 fish per tank, based on the number of fish received from other facilities and to assist in maintaining acceptable water quality. Colony fish were maintained on a 14-hour light cycle and were fed GEMMA 300 (Skretting, Maine, USA) as a total nutritional source 3 times daily, with rotifer supplements at noon.

3.2.3 Embryo Collection and Rearing

Breeding pairs were set up two hours prior to the beginning of the night cycle. One male and one female adult were transferred to a breeding tank containing 5 cm of system water. Females were bred no more than once per week. Eggs were collected the following morning, 3-4 hours after the beginning of the light cycle, and adults were returned to their respective tanks.

Harvested eggs were collected using a 25 mL serological pipette and a pipette pump (Catalog No. Bel-Art™ 13-683D, Fisher Scientific). Eggs were transferred to a 100 x 15 mm petri dish filled with 20 mL of system water. Using a stereomicroscope, fertilized eggs were identified by the presence of a cell cluster within an unblemished chorion (Figure 3.1). Unfertilized eggs and surplus embryos were transferred to a 5% Bleach solution for 5 minutes prior to disposal as biohazardous waste.

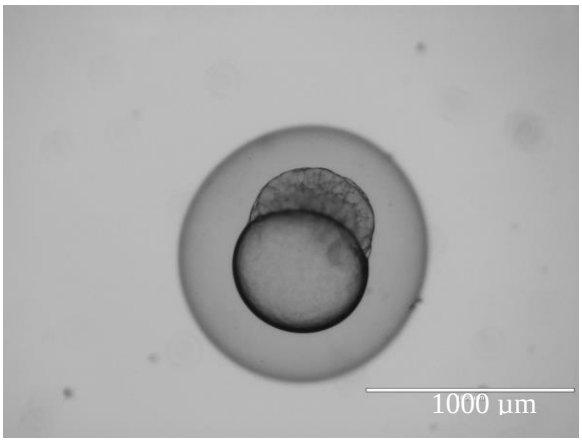

Figure 3.1: An example of fertilized zebrafish egg. The egg was imaged 2 hours post fertilization, with the yolk sac and blastula visible within the outer chorion.

Viable embryos were transferred to a new 100 x 15 mm petri dish filled with 20 mL of system water at a maximum density of 20 eggs per petri dish and maintained at 28.5 ^{o}C. Embryos were checked twice daily and any non-viable embryos were removed, bleached (5% bleach solution for 30 minutes) and disposed of as biohazardous waste. By 3 dpf,

embryos had naturally dechorionated. After 5 dpf, embryos were provided Gemma Micro 75 (Skretting) as an independent food source.

3.2.4 Zebrafish Euthanasia

Euthanasia of zebrafish larvae, juveniles, and adults were performed via hypothermic shock [34, 103]. Briefly, embryos were deposited into a 5:1 ice to water mixture and left at 4 ºC for a minimum of 30 minutes. Death, indicated by a lack of heartbeat, was confirmed via microscopy.

3.3 Microneedle Pulling and Beveling

Microinjection needles were created by pulling borosilicate capillaries (Catalog No. 1B100-4, WPI, Florida, USA) using a PUL-1000 4-step needle puller (WPI). A variety of pulling programs were developed to produce appropriately shaped needles, as described in 4.2.1. Once an appropriate program was identified, pulling parameters were kept consistent for all needles used for microinjection, regardless of desired size of microparticle to be injected. This was achieved by creating a long taper and a sealed needle tip approximately 1 µm in diameter.

Pulled microneedles were then beveled using a BV-10 beveller, equipped with a 104C diamond grinding plate (Sutter Instruments, California, USA). Beveling was necessary to create a smooth orifice in the tip of the needles (as opposed to manually breaking the needle tip with forceps or razor blade). The desired microneedle orifice was targeted to be diameter of twice that of the microparticle size. Briefly, the pulled microneedle was set into a needle holder angled at 45 ° off the horizontal. Once set, 5 mL of water was put onto the surface of the rotating grinding plate to better visualize the beveling, reduce the

chances of airborne debris, and minimize heat generation. The needle was lowered to the surface of the water using a coarse adjustment knob. Once the surface of the water was broken by the tip of the needle, it was lowered an additional 4 - 6 mm, (Table 3.1) until the needle surface is worn away to create the desired orifice diameter. This point was observed by water aspiration into the needle, due to the capillary forces caused by the rotating beveling stage and the micron scale opening in the needle tip. Once the breaking of the tip occurred, the needle was kept at a constant depth for 30 seconds, and was then raised from the surface of the water and removed from the needle holder.

Table 3.1: Beveling depths, measured from the height at which the unbeveled needle tip breaks the surface of the water film on the beveling surface, and associated needle orifice size used for needles for injections of various microparticles.

Depth (mm)	Orifice Size (µm)
4	20
5	50
6	100

Beveled needles were flushed with air to remove excess water and debris from the needle tip that were collected during the beveling of the microneedle. After flushing, the beveled needles were dried at room temperature for a minimum of 24 hours before use.

3.4 Microparticle Injection in Zebrafish Larvae

The development of a successful platform for the injection of microparticles into zebrafish embryos involved the generation of an injection stage, an anesthetic solution, and determination of an appropriate age range for injection.

3.4.1 Development of Injection Stage

An injection stage with microparticle reservoir was prepared to position and hold the zebrafish embryos for microparticle implantation, as described in Gerlach *et al.* [104]

with slight modification. Briefly, 0.5 g of agar (Cat No. BP1423-500, Fisher Scientific) was added to 25 mL of reverse osmosis (RO) water, , and heated in a boiling water bath for 5 minutes, or until the agar was completely dissolved. The lid of a 35 x 10 mm petri dish was held down on the bottom of a 100 mm x 15 mm petri dish, and 25 mL of the 2% agar solution was slowly poured into the bottom of the larger petri dish (Figure 3.2). Once cooled, the agar was covered in 10 mL of RO water to prevent dehydration and the larger petri dish was sealed with Parafilm and stored at 4° C until use.

Figure 3.2: An injection stage, with a 35 x10 mm dish acting as microparticle reservoir, for positioning anesthetized embryos during microparticle injection.

3.4.2 Microparticle Preparation

10 µm diameter poly(styrene) microparticles labeled with 4',6-Diamidino-2-Phenylindole, Dihydrochloride (DAPI) were purchased from Thermo Fisher Scientific (Cat No. F8829). Microparticles were received in suspension. For injections, the suspension was diluted in ultra-pure water (MilliQ ZRXQ003CA, Millipore, Ontario, Canada) to a final concentration of 1 vol%. Poly(ethylene) microparticles labeled with Texas Red were purchased from Cospheric LLC (California, USA) with nominal diameters of 50µm (UVPMS-BR-1.090 45-53 µm, lot 1407107-1) and 25µm (UVPMS-BR-0.995 22-27 µm, lot 150702-1). Microparticles were received as a dry product. For

injections, microparticles were suspended at 10 wt% in ultra-pure water (MilliQ). After suspension, microparticles stored at 4 ºC, protected from light, and used over the course of 4 months.

To enhance the hydrophilicity and improve handling of microparticles, bovine serum albumin (BSA) (Cat. No. FERB14, Fisher Scientific) was added to the microparticle suspensions to a final concentration of 0.1 mg/mL of BSA in the microparticle suspension. After addition of BSA, the solution was vortexed for 5 minutes and then incubated at 37 ºC for 30 minutes before being stored at 4 ºC. The microparticle suspensions with BSA was used over the course of 4 months. Prior to use, all microparticle stock suspensions were vortexed for 30 seconds to ensure uniform distribution of microparticles.

All microparticle suspensions were tested for endotoxin contamination prior to injection using a LAL Pyrochrome Kit (Cat. No. C1500, Associates of Cape Cod, Massachusetts, USA), per the manufacturer's instructions. Briefly, microparticles were suspended at 10 wt% in endotoxin-free water (EFW), and incubated at room temperature for 1 hour. The supernatant was then collected for endotoxin testing. A standard curve (2.5 endotoxin units (EU)/mL to 0.05 EU/mL in EFW) was prepared. EFW was used as the negative control, while a "spike-in" of control standard endotoxin at 0.25 EU/mL into a microparticle sample was used as a positive control. 50 µL of each standards, controls and samples were added to a 96 well-plate in triplicate. 50 µL of Pyrochrome reagent was added to each well, and the plate was covered and incubated at 37° C for 27 minutes. After incubation, the Pyrochrome reaction was halted by addition of 25 µL of 50 vol% acetic acid in EFW and the optical density was measured at 405 nm. Based on the

standard curve, all microparticle suspensions had endotoxin concentrations below detectable levels (0.05 EU/mL).

3.4.3 Preparation of Anesthetic Solution

Tricaine (Cat. No. A5040, Sigma-Aldrich) was used to anesthetize zebrafish embryos and larvae prior to injection. A buffered 25 mg/mL stock solution of tricaine was prepared fresh weekly by adding 100 mg tricaine and 0.575 mL 1M Tris Buffer (Cat. No. RDD008, Sigma-Aldrich) to 25 mL of RO water. The stock solution was stored in a Parafilm-sealed vial at -20 ºC for up to 1 week. A working solution of tricaine (1.05 mg/mL) was prepared immediately prior to injections by diluting 0.84 mL of 25 mg/mL stock solution in 20 mL of system water. This working solution concentration anesthetized embryos within 20 seconds of exposure, and recovery of normal nervous function was achieved within 10 minutes of removal from the anesthetic solution.

3.4.4 Microinjection of Zebrafish Larvae

Microparticle injections were performed under a standard stereomicroscope using an Eppendorf Oil/Vario manual microinjector (Eppendorf, Ontario, Canada) and a 3-axis manual micromanipulator. An overview of the workflow is provided in Figure 3.3.

Injection studies were performed with three test groups: a tricaine exposure group, a vehicle only injection group, and the microparticle implantation group. For the tricaine exposure group, embryos were placed on the agar injection stage in the buffered tricaine solution for 20 minutes, then were transferred to a dish containing system water. The vehicle only injection group was anesthetized then received injections of the vehicle solution (0.1 mg/ml BSA in system water). The microparticle implantation group was

anesthetized then injected with microparticles in the vehicle solution. While injection of single microparticles was targeted, a small number of fish did receive up to 5 microparticles.

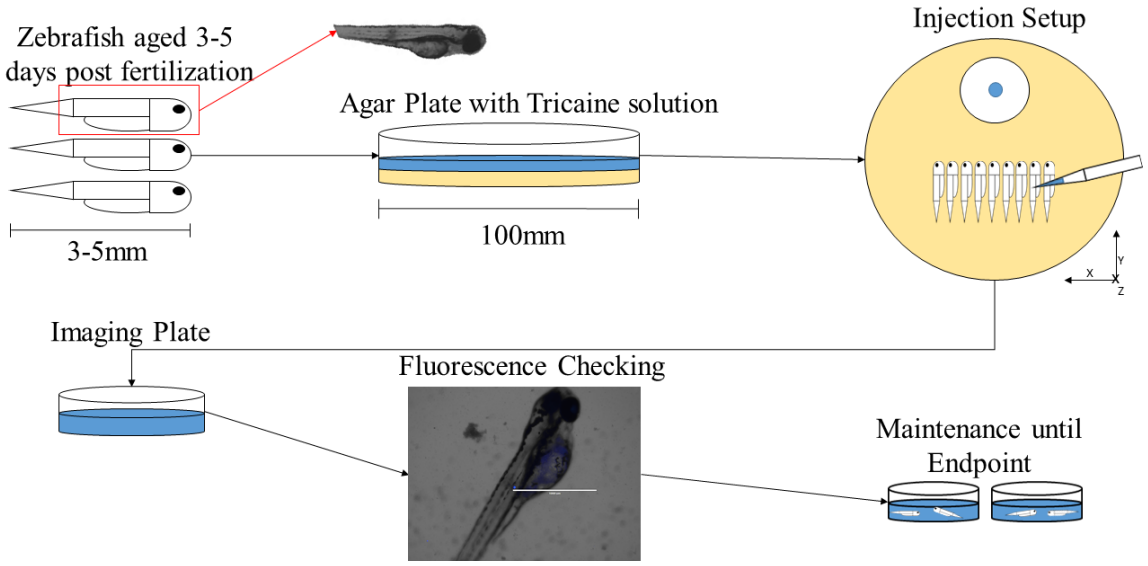

Figure 3.3: Workflow diagram of the injection and recovery process. Zebrafish were transferred to the injection stage and covered in tricaine anesthetic solution. Single microparticles or the vehicle solution were aspirated and injected into the trunks of 3 – 5 dpf zebrafish embryos. After injection, embryos were transferred to an imaging plate filled with tricaine anesthetic, and the implant success was visually determined by fluorescent microscopy. Embryos were then sorted into recovery dishes containing fresh system water, and maintained until respective endpoints.

Once the fish were anesthetized, microparticles were aspirated from the microparticle reservoir into the beveled microneedle. The microneedle was then positioned above the embryos, and lowered until just above the surface of the tricaine solution. Once above the surface of an embryo trunk and the "piercing" axis was used. This axis is rotated 45 ° from horizontal, and was actuated downward along a combined z and x axis. Implantations were performed by turning the fine adjustment knob on the microinjector until a microparticle was observed leaving the needle tip. After injections, embryos were transferred to the imaging plate and remained stationary until all embryos were injected

and transferred. The imaging plate was transferred to an observation stage of a fluorescent microscope (EVOS FL, Thermo Fisher Scientific, Ontario, Canada). Injected embryo viability was first checked using transmitted light to observe a heartbeat. Once viability was established, the relevant fluorescent channel was chosen to determine if injections were successful. Embryos were then transferred to their respective recovery dishes and allowed to recover in system water at 28 ºC within an incubator (Thermo Fisher Scientific) before imaging at later time points.

3.5 Histological Analysis of Zebrafish Embryos

3.5.1 Fabrication of custom zebrafish-array mold

Histology was performed on zebrafish to examine embryonic and larval tissue around microparticle implants. Due to the small size of the embryos (typically 5 – 10 mm in length, and 1 – 2 mm in diameter), handling of embryos as individual specimens proved technically challenging throughout the histology sample preparation process, and precluded the use of an automated processor. To address this limitation, a custom mold was designed, in collaboration with Dr. Carlos Escobedo and Dr. Reza Nosrati (Chemical Engineering, Queen's University, Ontario, Canada), to generate an embryo array in an agar template, similar to that previously described in Sabaliauskas *et al.* [66] . The master mold was designed using SolidEdge software (v. 7, Siemens, Munich, Germany) and was 3D printed using a MiiCraft plus 3D printer out of Miicraft resin (Catalog No. Clear resin BV-003, lot 1510-2, Miicraft, Jena, Germany) (Figure 3.4).

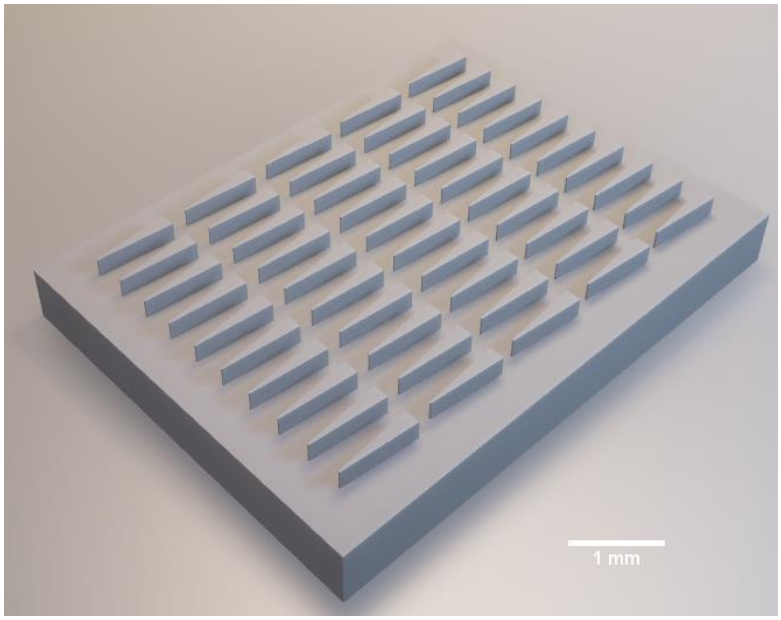

Figure 3.4: The isometric view of the final CAD drawing for the agar mold, which was 3D printed to work with zebrafish embryos in an automated processor.

Agar templates containing an array of wedge-shaped holes were made by pouring molten 2% agar into a 100 x 15 mm petri dish. Once cooled to a semi-solid state, the master mold was pushed into the agar and left until the agar had fully solidified. After solidification, the master mold was removed from the surface, and the agar mold was cut out from the surrounding agar.

3.5.2 Histology Protocol Development

Following euthanasia, embryos were transferred to 15 mL conical tube containing a 10% neutral buffered formalin solution (Cat. No. SF100-4, Fisher Scientific) and stored at 4 ºC for 2 hours to overnight. Different formalin incubation times were trialed to obtain the appropriate fixation protocol of 2 hours for zebrafish embryos and larvae. After fixation, zebrafish were stored in a 70% ethanol solution in RO water for a minimum of 1 hour, or a maximum of 7 days prior to embedding embryos in the custom agar tissue-array template. Embryos were added to the agar template, and positioned into slots. After properly positioning the embryos, a 2% agar solution was gently pipetted on top of the

agar template to seal the embryos in place. The template was cooled prior to submission to the Queen's Laboratory for Molecular Pathology, where embryo arrays were dehydrated using ethanol and xylene rinses and embedded in paraffin by Dr. Lee Boudreau.

Paraffin-embedded embryos were sectioned using a HM 355S microtome (Cat. No. 905200, Thermo Fisher Scientific) with MX 35 Premiere+ blades (Cat. No. 3052835, Thermo Fisher Scientific). Blocks were serial-sectioned at thicknesses of 7 µm, and ribbons were made of at most 5 sections before being transferred to a hot water bath at 45 ºC. Once sectioned and placed onto microscope slides (Cat. No. 12-550-15, Fisher Scientific), slides were put into a dry oven at 60 ºC for 1 hour. Sections were stained using a progressive Gill 2 hematoxylin (Cat. No. 28-601-08, Fisher Scientific) and eosin (Cat. No. SE23-500D, Fisher Scientific) (H&E) stain. Slide-mounted tissue sections were deparaffinized and rehydrated using a series of D-Limonene (Cat. No. 89370-092, VWR, Ontario, Canada) and ethanol solutions prior to H&E staining, dehydrating and sealing with a D-Limonene based resin. Briefly, slides were soaked in D-Limonene (3 x 4 minutes), passed through an ethanol dilutions series (100%, 85% and 70% in water, dipping slides 12 times in each ethanol solution) and soaked in tap water for 5 minutes. Slides were stained with Gill 2 Hematoxylin for 2 minutes and then soaked in tap water for 5 minutes. Slides were then transferred to 90% ethanol for 1 minute before being counterstained in 10% Eosin for 90 seconds. The stain was differentiated in 90% ethanol for 90 seconds. After differentiation, the tissues were dehydrated by reversing the previous rehydration step, beginning with 70% ethanol and ending with 100% D-Limonene. After dehydration, slides were sealed with a coverslip in D-Limonene based

resin (Cat. No. O8015, Sigma-Aldrich) and dried for 24 hours. Imaging of H&E stained section was performed using a bright field microscope with color camera (EVOS XL, Thermo Fisher Scientific).

3.6 Statistical Analysis

The standard error of the proportion (SEP) was calculated for the success and retention percentages for each condition. The SEP and sample size were then used in a one-way analysis of variance (ANOVA) with Tukey post-hoc multiple comparison analysis. Prism software (v 5.01, Graphpad, California, USA) was used for the one-way ANOVA and Tukey post-hoc test.

Kaplan-Meyer survival curves were generated using Prism software (Graphpad). Statistical analysis of survival curves was performed using the Log-Rank test. Embryos that were intentionally euthanized as an experimental endpoint were denoted as "censored" subjects, and were not considered as measurements of loss in viability.

Chapter 4

Results and Discussion

4.1 Biomaterial Implant Model Development in Zebrafish Embryos and Larvae

Zebrafish possess many advantages as a model organism, such as optical transparency, high fecundity and simple egg collection due to external fertilization [34]. However, there are also several technical challenges that were addressed in the development of a protocol for solid polymer microparticles implantation. These included the small size of zebrafish embryos and larvae that necessitated the use of microinjection techniques for microparticle implantation, changes in the physiological properties of zebrafish as they transition from egg to adult, and the natural die-off periods present within the developmental cycle.

To support the development of a zebrafish implant model, a zebrafish colony was established at Queen's University to provide a consistent source of zebrafish embryos. First, a population of wild-type Tübingen (TU) zebrafish was established, and these TU adults were used to generate the embryos used in this study. More recently, transgenic zebrafish with GFP-labeled macrophages *Tg(mpeg: eGFP)* and neutrophils *Tg(mpeg: eGFP)* were introduced into the colony, enabling transgenic embryo collection for preliminary fluorescence microscopy examination of microparticle injections.

4.1.1 Selection of developmental stage for injection

To develop a reproducible model for microparticle implantation in zebrafish embryos, the early development of zebrafish was examined to identify an appropriate injection window. Upon collection at approximately 2 hours post fertilization (hpf), zebrafish

embryos consisted of a collection of 32 to 64 cells enclosed within a protective chorion (Figure 4.1a). Natural dechorionation of embryos consistently occurred by 3 days post fertilization. Prior to dechorionation, targeted injection was technically challenging as these embryos were tightly curled upon themselves. Piercing the chorion itself was also challenging, as it tended to roll under the pressure of the piercing microneedle. Finally, the innate immune system develops between 2 and 3 dpf [25]. Consequently, injections prior to 3 dpf may increase the variability in the observed responses to implanted materials (Figure 4.1b). The upper limit for embryonic injections was determined to be 5 dpf, as the development of scales in wildtype zebrafish after this time point impeded the use of borosilicate microneedles (Figure 4.1c) [71].

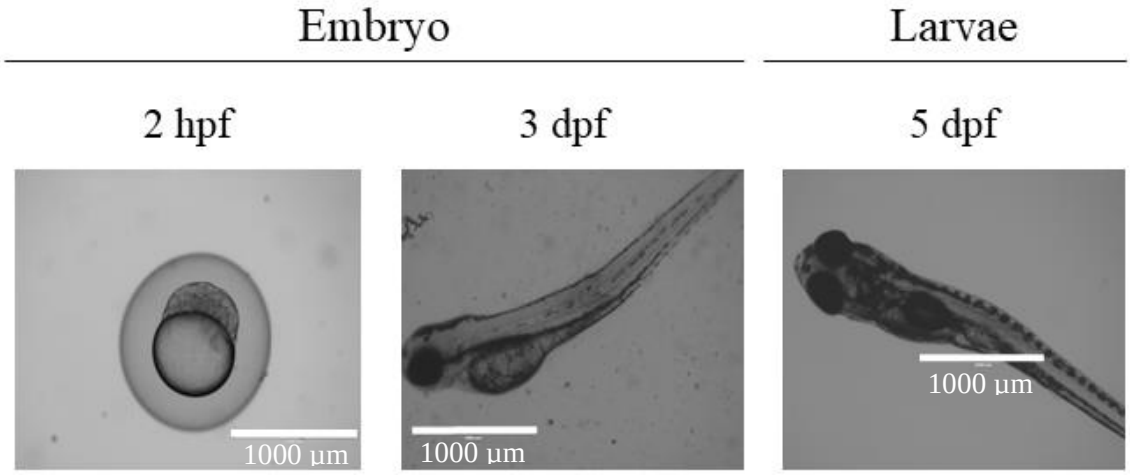

Figure 4.1: Representative images of relevant zebrafish stages of development. At 2 hpf, a thick chorion enclosed the developing embryos, which consisted of a yolk sac and rapidly dividing cluster of cells. By 3 dpf, embryos had hatched from the chorion and were approximately 3 mm in length. Distinct anatomical features were apparent, including the head, eyes, yolk sack and trunk. At 5 dpf, the embryo has increased in length to 5 mm, and the yolk sac was visibly reduced, with a rudimentary gut system taking its place. Additionally, pigmentation begins developing along the trunk of the zebrafish, marking its transition to a larva.

Furthermore, embryos began to develop pigmentation along the trunk of the larvae after 5 dpf, which interfered with visualization of the implants in wildtype embryos. Based on

these collective observations, the range of 3 - 5 dpf was targeted for microparticle injection by pulled borosilicate microneedles. Given the high fecundity available to zebrafish and the ability to perform injections with disposable, borosilicate needles, the three day injection window provided ample time to perform upwards of 30 manual injections per week.

4.1.2 Natural die-off periods

The natural developmental cycle of zebrafish included an observed series of natural die-off points, as zebrafish progress from the embryonic to juvenile stages. Embryos reared within the Queen's colony demonstrate two main die-off periods that occur at approximately 24 hpf, and between 12-15 dpf. The 24 hpf die-off period was attributed to poor fertilization and genetic defects [34]. The embryo loss during this early die-off period was highly variable, with an average mortality of 25%. However, some instances of 100% mortality were observed. The early die-off period was consistent with experiences at other zebrafish colonies, although reported die-off rates were as low as 23% [105]. The second natural die-off period occurred between 12 and 15 dpf. At this point in zebrafish development, the gut system is the sole source of nutrition, and the nutritional demands increase dramatically as the zebrafish begin increasing their size and activity level [70]. While the percent of embryos lost due to the natural die-off periods in development vary among breeding events, it was determined that collecting and rearing 33% excess embryos was recommended to account for the initial 24 hpf die-off period. In experiments that extend beyond 12 dpf, an additional 10% should be included in experimental condition replicates to account for the expected loss of fish during the second die-off period.

4.2 Microneedle Pulling and Beveling

4.2.1 Microneedle Pulling Programs

In addition to determination of an appropriate age range for microparticle injections during the embryonic/larval stage, it was necessary to establish microneedle pulling and beveling parameters to obtain appropriate needle shapes and sizes for microparticle injections. Several factors were determined to play critical roles in injection, and needle pulling was adjusted to improve these factors. The microneedle taper length and tip diameter was tuned by adjusting the following parameters on the microcapillary puller: heating temperature, pull distance, pull force, and delay between pulling steps (Table 4.1).

Table 4.1: Microcapillary pulling parameters and associated effects on final microneedle taper and tip size.

Pulling Parameter	Effect on needle shape, if increased
Heating temperature	Longer, finer taper
Pull distance	Smaller tips
Pull force	Smaller tips
Delay between steps	Shorter taper

Furthermore, pulling programs that involve multiple steps can be used to fine-tune needle shape and size. For microparticle injection, a needle with a long taper and relatively large microinjection needle tip was desired (when compared with microneedles pulled for the injection of solutions) to accommodate the aspiration and ejection of microparticles with 10 – 50 μm diameters. Therefore, a final pulling program was developed to produce both a long taper and a final unbeveled needle size of 10 μm or less. Establishing a consistent initial microneedle shape enabled the application of a simplified beveling protocol for

obtaining needle orifices of varying diameters to accommodate a wide range of microparticle sizes.

Based on the relationship between parameters, three initial programs were developed and the resulting microneedle shapes were compared (Table 4.2). A detailed description of the three pulling programs is provided in Appendix A. A final pulling program was selected based on desired traits. Pulling program "A" generated needles with a short taper (1600 um) and a relatively large tip (approximately 10 μm). While this large microneedle tip allowed for faster beveling of larger needles, the short taper caused rapid changes in the orifice diameter with small changes in bevel height. This coarse control made targeting a desired final needle bore opening difficult. Pulling program "B" was a modification of Program "A", in which the pulling force and the delay between pulling steps were increased, but the heat and distance were decreased. As expected, these parameters changes produced a needle with a larger final tip size (50 um) and shorter taper (1200 um), compared to program "A". While the large tip reduced the overall bevel time necessary obtain a large (i.e. 100 μm) opening, these needles were too large for the injection of microparticle under approximately 50 μm in diameter. In pulling program "C", the heating temperature and the pulling distance per step was maximized based on program "A". This program produced microneedles with a long taper (2000 μm) and tip size of approximately 1 μm. The long taper provided the equivalent of a fine control on beveling, while the fine tip allowed for needles to be used for microparticles of all sizes used for this study. As this pulling program produced needles with the desired shape and size, it was selected to produce microneedles used in microparticle injections.

Table 4.2: The representative images and results of the three pulling programs used to produce microneedles. Representative images are included for each program.

Program	Needle	Taper length	Tip size	Notes
A	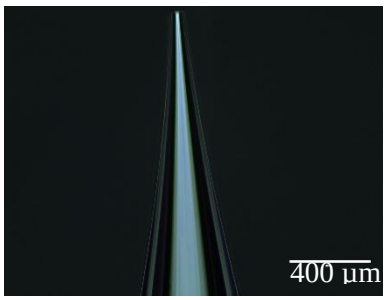	1600 µm	10 µm	Short taper caused rapid changes in the orifice diameter with small changes in bevel height
B	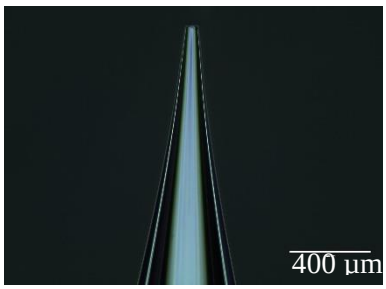	1200 µm	50 µm	Needle orifice was too large for tight control of small (10 µm) microparticles
C	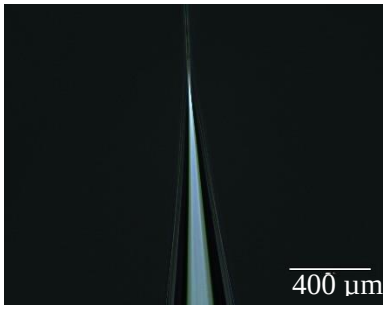	2000 µm	1 µm	Long taper provided excellent control of orifice diameter during beveling. Small needle tip accommodated for all microparticle sizes

4.2.2 Microneedle Beveling

After needle pulling, needle tips were beveled to obtain orifices of specific diameters and bevel angles. While it is possible to break the needle using a straight razor, this can lead to variable needle tip diameter and jagged orifices, which affects the aspiration and injection of microparticles. Beveling, however, provides consistent needle openings, with well-defined and smooth piercing edges (Table 4.3). For this work, initial orifice to microparticle diameter ratios were targeted at 2 to 1. This initial selection was to ensure

that aspiration of microparticles could be performed with ease, while simultaneously reducing the chance of clogging within the microneedle.

It was observed that some beveled needles had a non-uniform grinding edge, such as the 50 μm bevel size imaged (Table 4.3). This was believed to be caused by a wearing down of the diamond grinding plate over time, and can be addressed by adjusting the point on which the needle is beveled for future microneedles. However, this wave pattern still provided an adequate piercing point. Variations in bore size for injections were minimized by eliminating needle bore sizes that were 5 μm larger or smaller than the targeted size.

The three bore sizes (20 μm, 50 μm and 100 μm), and their associated microparticles (10 μm, 25 μm and 50 μm, respectively), were used for injections into zebrafish embryos as described in 3.4.4. Needles were used for an average of 5 injections before being replaced with a fresh needle. While clogging with microparticles was minimal, debris from zebrafish tissue did accumulate in the needle tip and resulted in needle clogging after repeated injections.

4.3 Microparticle Injection in Zebrafish Larvae

Commercially available, fluorescently-labeled polymer microparticles with diameters ranging from 10 – 50 μm (Table 4.3) were injected into the trunks of 3 – 5 dpf zebrafish larvae to assess injection success rates, larvae survival and microparticle retention rates, as a function of microparticle diameter. Microparticle materials were selected based on criteria described in 2.4.1. All of the data in this section reflect the cumulative injections that were performed over the 32 weeks of the study.

Table 4.3: The microparticle diameter and beveled needle orifice used for microparticle injections in zebrafish embryos, with representative images of the microparticles and beveled needles.

Microparticle Size, Polymer, and Marker		Beveled Needle Orifice	
10 µm, Poly(styrene), DAPI marker	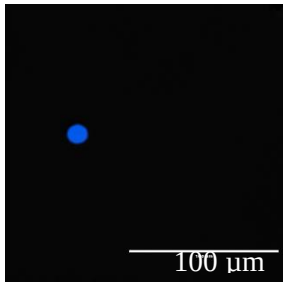	20 µm	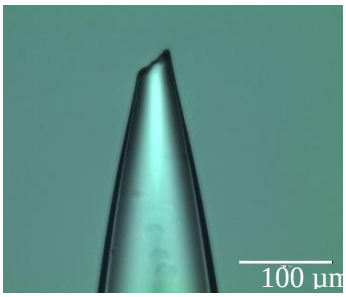
25 µm, Poly(ethylene), Texas Red marker	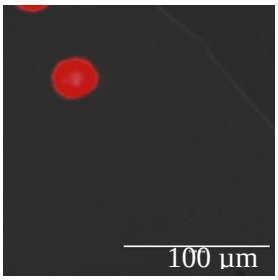	50 µm	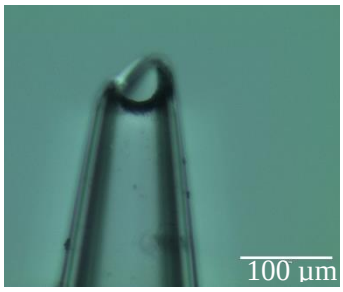
50 µm, Poly(ethylene), Texas Red marker	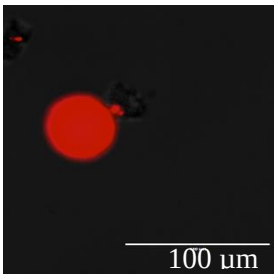	100 µm	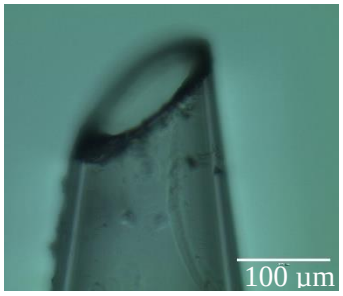

4.3.1 Implantation Success Rates

The implantation success rate was defined as the number of successful injections (i.e. number of zebrafish with an implanted microparticle) per total attempted injections, measured immediately post injection (Figure 4.2). The highest success rate was observed with the 10 µm microparticles at 33%, while the 25 and 50 µm microparticles had success rates of 16% and 11%, respectively.

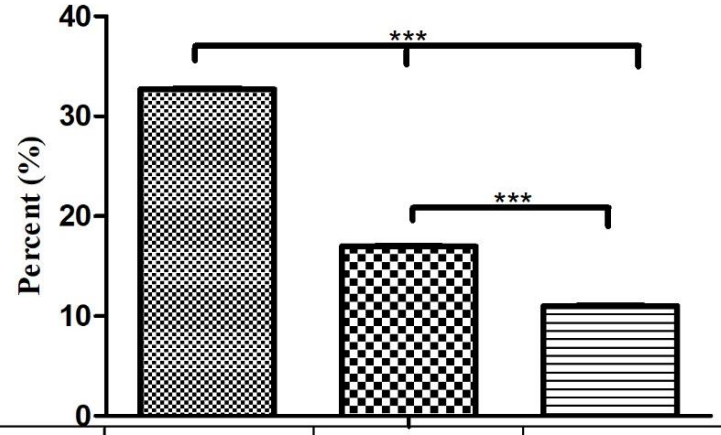

Size of Microparticle (μm)	10	25	50
Number of Total Injections	55	53	77
Number of Successful Injections	18	9	9

Figure 4.2: The implantation success rates as a function of microparticle diameter. Injection success was determined by visual confirmation of an implanted microparticle immediately post injection. A summary table of the number of replicates for each condition is listed below the graph. Data represented as percent success ± SEP, ***p<0.0001 determined via a one-way ANOVA and Tukey's post-hoc multiple comparisons test.

The success rates had low standard errors of proportion (SEP) due to the large number of replicates for each microparticle size (10 μm diameter: n =55, SEP = 0.063; 25 μm diameter: n = 53, SEP = 0.052; 50 μm diameter: n = 77, SEP = 0.037). One-way analysis of variance (ANOVA) with a Tukey post-hoc test determined that microparticle diameter had a significant effect on implant success rates ($p < 0.001$). This suggested that increasing microparticle sizes resulted in decreased success rates for the given microparticle range tested.

While the observed success rates were lower than expected, large numbers of zebrafish embryos can be obtained with relative ease and low cost, compared to rodent models [34]. Therefore, sufficiently large numbers of implant replicates could be achieved by increasing the total number of attempts, despite the low success rates. Furthermore, it

may be possible to improve implant success rates with further refinement of injection techniques, such as using a smaller needle bore to microparticle ratio.

4.3.2 Implantation Retention

While success rates were measured immediately following implantation, we also observed an unexpected loss of implanted microparticles following the initial 24 hour period. Consequently, the retention of microparticles within the implant site beyond 24 hours post implant (hpi) was investigated as a function of microparticle size. Microparticle retention was defined as the percent of successful implants that remained present within the implant site 24 hpi (Figure 1.9). Retention measurements were only performed with the successful implantations, with each group having greater than 6 replicates. While microparticles with smaller diameter (10 and 25 μm) had retentions of 78%, the large 50 μm microparticle implants had only 11% retention. Furthermore, statistical analysis demonstrated a significant difference between the 50 μm microparticles and the two other groups ($p < 0.0001$). This suggested that, unlike success rates that decreased with increasing microparticle diameter, retention of the 50 μm microparticles was particularly problematic. The expulsion of microparticles may have occurred through either a passive or active mechanism. The passive mechanism describes a process in which the microparticle works its way out of the wound, along the injection path, based on its relative size and location to the wound site. The active mechanism, however, is described by an immune response, in which fibrous tissue forces the microparticle to the surface of the skin, and eventually expels it, similar to a splinter in humans [57].

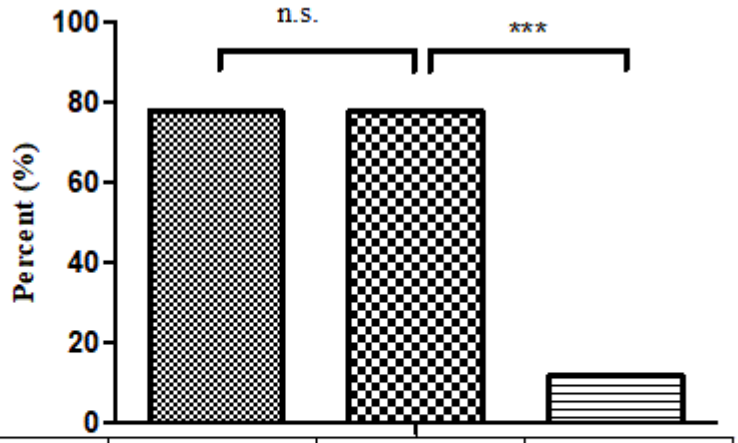

Size of Microparticle (µm)	10	25	50
Number of Successful Injections	18	9	9
Number of Retained Microparticles	14	7	1

Figure 4.3: Retention rates after 24 hpi. Retention rates were determined by examining the implants 24 hpi. Implants that were no longer present were considered "lost". A summary table of the microparticle size (µm), initial successful implants and number of microparticles retained after 24 hpi. Data represented as percentage ± SEP, ***p<0.0001 determined via one-way ANOVA and Tukey's post-hoc multiple comparisons test.

The active mechanism of expulsion has been observed in other fish models, such as catfish, in which a fibrous formation developed internally to the implant (such as a tracking device) and slowly forced the implant out through the surface of the skin, at a location distant from the original implant wound [57]. In our study, one microparticle expulsion event was partially captured by microscopy, demonstrating the movement of the particle from the initial implant location (2 hpi) to the surface of the zebrafish (24 hpi), before it was expelled from the tissue and no longer visible within the wound site (26 hpi) (Figure 4.4).

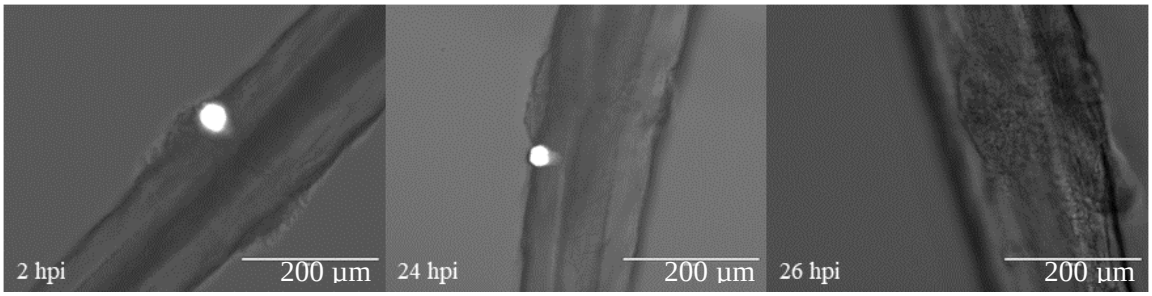

Figure 4.4: A time series of microparticle expulsion over 26 hpi in a *Tg(mpeg: GFP)* zebrafish embryo. The white dot represents a 25 µm PE microparticle labelled with Texas Red.

Retention was discovered to be a major issue in larger implants as experiments continued. Loss of microparticles post implantation enhanced the already low success rates when attempting to assess viability out to 30 dpi. Similar to low injection success rates, microparticle retention numbers, can be increased by increasing the number of injections performed. However, the combination of low retention and implant success observed with the 50 µm microparticle size suggested that the implant or associated wound size may be too large, and are not acceptable for implantation in zebrafish embryos. It may be possible to improve retention rates by decreasing the needle orifice (and therefore, wound size) used to inject the 50 µm particles. Alternatively, the use of a tool to position the implanted microparticle deep within the implant site post injection should also be explored as a method to improve retention. A similar technique was described by Gerlach *et al*., where a whisker tool was used to position 50 - 100 µm beads within the developing zebrafish yolk sac [104].

4.3.3 Survival Rates of Injected Fish

One of the key goals in developing the zebrafish microinjection platform was to identify acceptable implant sizes and needle bore sizes that avoid significant reduction in viability of implanted or injected zebrafish embryos. To examine this, survival curves were

generated for each injection condition (i.e. microparticle vs vehicle only), as well as for zebrafish larvae exposed only to the anesthetic tricaine. Fish that received an implant, but then did not retain their implants, were tracked as successful implants out to 30 days and were not censored. The following data were generated using Tübingen strain wildtype zebrafish embryos.

4.3.3.1 Survival Rates with 10 µm Diameter Microparticle Implantations

The first condition examined was the 10 µm injection group. Injections were performed with 10 µm DAPI-labeled poly(styrene) microparticles suspended in 0.01 wt% BSA in water (Figure 4.5). The associated needle bore size was kept constant at 20 µm.

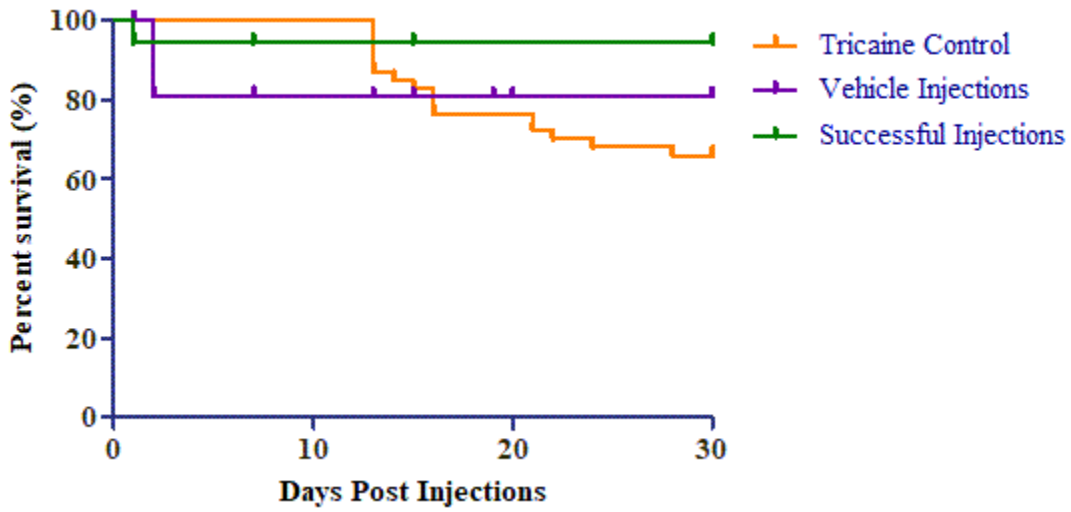

Figure 4.5: Survival curves for 10 µm poly(styrene) microparticle injections. Vehicle injections refer to sham injections that received high purity water and 0.01 wt% BSA, and successful injections refer to embryos that received a single implant. Tick marks denote sacrifice points, whereas changes in height represent unintended embryo death. No significant differences were observed between the three test groups, n = 47 for tricaine control, n = 35 for vehicle control, and n = 18 for successful injections.

Zebrafish larvae that received 10 µm microparticle or vehicle injections had high viability, with no deaths occurring after 3 dpi. When compared to the tricaine exposure group, no differences among the three groups were identified ($p > 0.05$). This suggests

that the 10 µm implants, as well as the wounds from the 20 µm needle bore, did not cause a significant reduction of viability in zebrafish embryos aged 3 to 5 dpf over the 30 dpi period. Furthermore, no morphological or behavioral variations were observed in embryos that received an implant or a vehicle injection, compared to zebrafish that were only exposed to anesthetic.

4.3.3.2 Survival Rates with 25 µm Diameter Microparticle Implantations

The next set of conditions tested was 25 µm poly(ethylene) microparticles labelled with Texas Red, injected with an associated needle bore size of 50 µm (Figure 4.6).

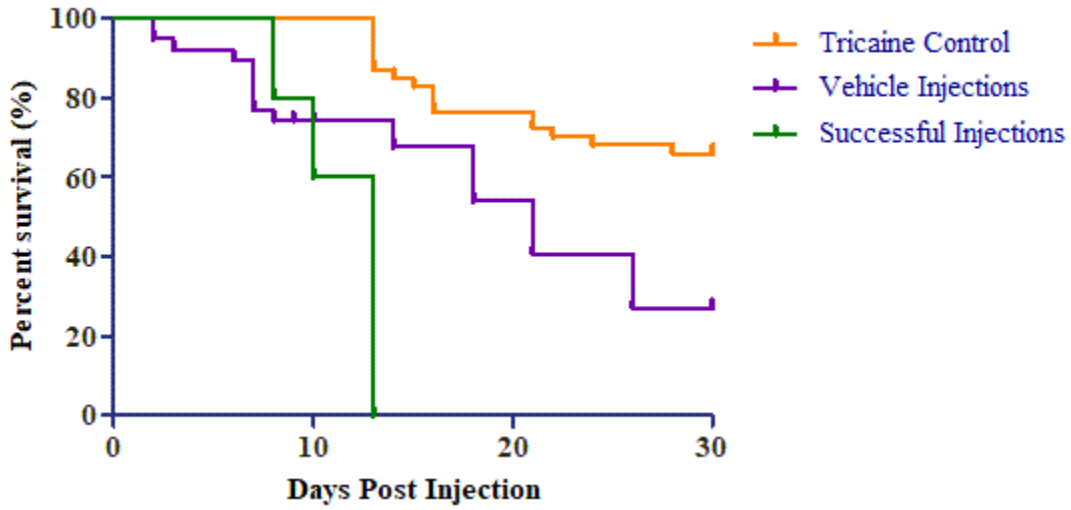

Figure 4.6: Survival curves for 25 µm poly(ethylene) microparticle implantations. Vehicle injections refer to sham injections that received high purity water and 0.01 wt% BSA, and successful injections refer to embryos that received a single implant. Tick marks denote sacrifice points, whereas changes in height represent unintended embryo death. Significant differences were observed between tricaine control and the other test groups ($p < 0.001$). No significant difference was observed between the vehicle control and successful injections. N = 47 for the tricaine control, n = 44 for vehicle injection, and n = 9 for successful injections.

From the survival curve, both the microparticle and vehicle injection group maintain a high survival rate up to 12 - 16 dpf. However, at 12 dpf the viability of the microparticle implant group decreases suddenly. While the difference in viability between successful

and vehicle control injection groups was not statistically significant ($p = 0.538$), the data suggests that the microparticle affects the survival of injected embryos, compared to vehicle control, at later time points. The lack of statistical significance could reflect the small size of the injection group compared to the vehicle injection group and it is possible that increasing the implant replicates would provide conclusive data. Additionally, reducing the bore size to microparticle diameter ratio may reduce the loss in viability in the implant test group. Future work should investigate this further. However, injections of 25 μm microparticle or vehicle using the 50 μm bore needles caused a significant decrease in viability, compared to both tricaine control ($p < 0.001$) and 10 μm implants ($p < 0.05$). Furthermore, there was no observed behavioral or morphological changes in injected embryos prior to death. This sudden death could be explained by a reduced ability to swim. At the observed die-off at approximately 11 dpf, which was similar to the natural die-off points during development, zebrafish nutritional requirements increase [31]. However, the presence of the microparticle in the muscle tissue could be decreasing the ability of the zebrafish to swim for its food. In future studies, it may be possible to examine this using a softer biomaterial, which would be expected to irritate the surrounding muscle tissue to a lesser extent.

4.3.3.3 Survival Rates with 50 μm Diameter Microparticle Implantations

The final injection condition used Texas Red-labeled 50 μm poly(ethylene) microparticles that were injected using a needle with a 100 μm bore (Figure 4.7). Injections using a 100 μm needle bore size significantly decreased the viability compared to the 50 μm bore size used in previous studies ($p < 0.0001$). Furthermore, implantation

of 50 µm microparticles further reduced viability, compared to the vehicle injections ($p < 0.0001$).

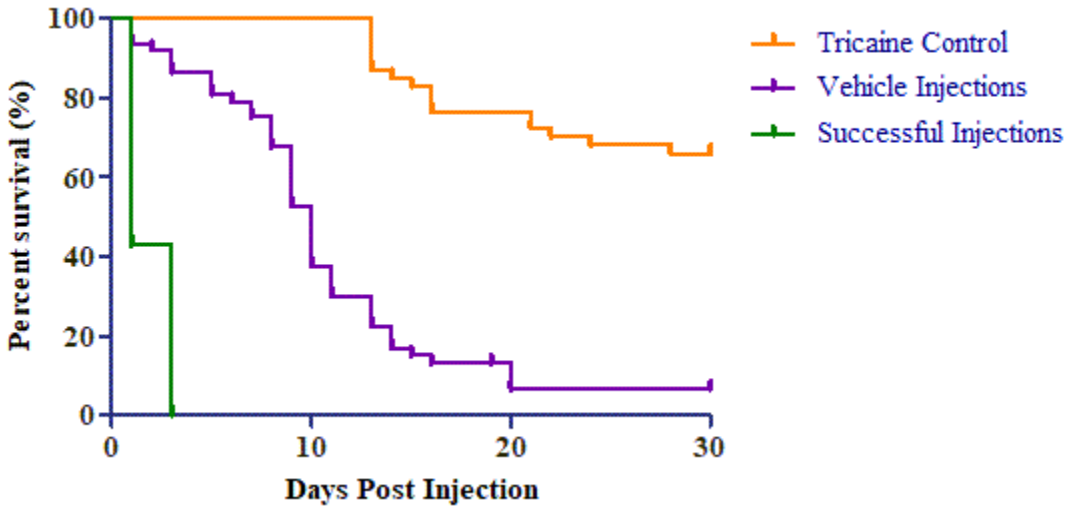

Figure 4.7: Survival curves of 50 µm poly(ethylene) microparticle injections using Texas red labelled poly(ethylene) microparticles. Vehicle injections refer to sham injections that received high purity water and 0.01 wt% BSA, and successful injections refer to embryos that received a single implant. Tick marks denote sacrifice points, whereas changes in height represent unintended embryo death. Significant differences were observed between all three test groups ($p < 0.0001$). N = 47 for tricaine controls, n = 68 for vehicle control, and n = 9 for successful injections.

Zebrafish embryos that received a single 50 µm microparticle did not survive past 3 dpi, suggesting that the combination of the 50 µm microparticle and 100 µm bore wound exceeded the acceptable injection conditions for zebrafish embryos aged 3 to 5 dpf. However, injection of 50 µm microparticles using a smaller needle bore should be investigated to determine if microparticles of this size may be better tolerated with a smaller wound. Based on the high mortality rate, poor implant success and poor retention, 50 µm microparticle injections were not pursued further within the scope of this thesis.

4.3.3.4 Effect of Needle Bore Size on Embryo Survival

In addition to comparing the survival curves of successful injections and vehicle controls within injection conditions, the effect of needle bore size on embryo survival was examined by comparing the survival curves for vehicle controls and the tricaine control group (Figure 4.8).

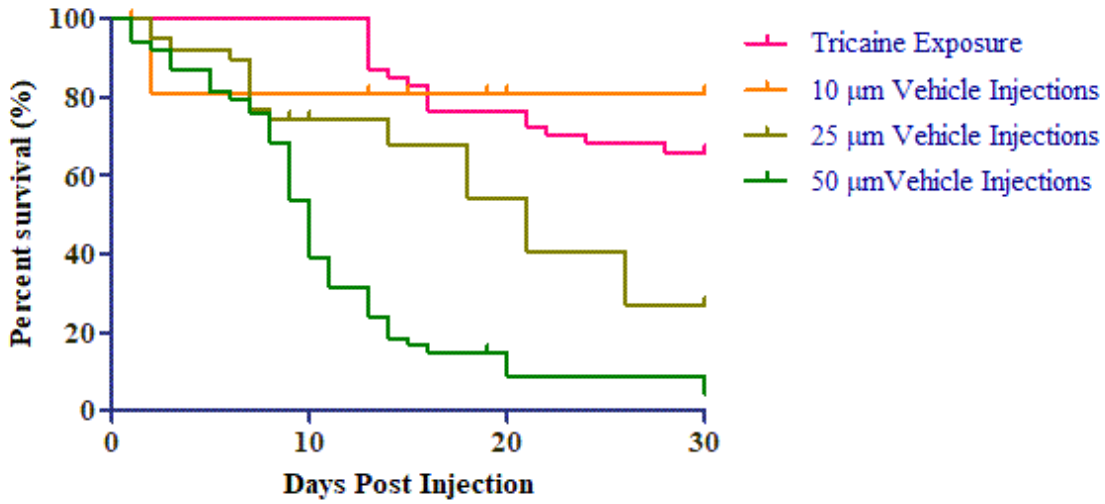

Figure 4.8: Effect of needle bore size on embryo survival. Vehicle injections refer to sham injections that received high purity water and 0.01 wt% BSA, which was compared to tricaine exposure groups. Tick marks denote sacrifice points, whereas changes in height represent unintended embryo death. Significant differences were observed between the tricaine exposure and the 25 and 50 µm injection groups ($p < 0.001$ and $p < 0.0001$, respectively). However, no significant differences were observed between the tricaine exposure and the 10 µm injection groups.

When survival curves for the three vehicle group were compared to specifically look at the effect of the needle bore size, it was apparent that the needle bore had a significant effect on larvae survival. There were no significant differences between 10 µm microparticle injection groups and tricaine control ($p = 0.9490$), indicating the wound size made with the smallest needle bore was well tolerated by the embryos. However, there were significant reductions in viability observed as the needle bore increased to 50 µm ($p = 0.0004$) and 100 µm ($p < 0.0001$), compared to the tricaine control group. These

data suggest that embryo viability may be improved by reducing the needle bore diameter. In this preliminary study, a needle bore twice the diameter of the microparticle was used. However, further experiments should be performed to determine the minimal clearance (i.e. difference in diameter) required for microparticle aspiration and injection without significant clogging, and the embryo survival using the reduced needle bore should be reexamined.

Another notable observation was that zebrafish yolk sacs exhibited auto-fluorescence at 450 nm while the zebrafish was anesthetized with tricaine. While the auto-fluorescence did fade following embryo recovery from anesthesia, this tricaine-associated auto fluorescence effect should be considered when selecting fluorophores and dyes for labeling microparticles in future work.

4.4 Fluorescent Imaging of Labelled Cells and Microparticles in Transgenic Fish Lines

A major motivation for using zebrafish as an animal model for assessing biomaterials is the ability to visualize and track cells *in vivo* using transgenic strains with fluorescently-labeled cell populations [35, 82]. In the context of host responses to implanted materials, the accumulation and persistence of neutrophils and macrophages at the implant site may provide a quantitative measure of the innate immune responses to, and therefore biocompatibility of, the implanted material. This was recently attempted, and both Zhang *et al*. and Witherel *et al*. demonstrated the ability to quantify early host immune response to implanted biomaterials [30, 32]. While the goal of Zhang *et al*. was to distinguish the host response to microparticle size and chemistry, the results were unconvincing, potentially due to the relatively similar microparticle diameters (10 and 15 μm) [30].

Two transgenic zebrafish strains with enhanced green fluorescent protein (eGFP) labeled macrophages *Tg(mpeg: eGFP)* and neutrophils *Tg(mpx: eGFP)* were procured by the Fitzpatrick zebrafish colony to explore the innate immune response in zebrafish using fluorescence microscopy. While logistical issues with procurement and breeding of these strains in the Fitzpatrick colony limited the availability of viable embryos (discussed below), some preliminary work with these strains was possible.

As expected, confocal examination of *Tg(mpx: eGFP)* embryos showed the presence of eGFP-labeled cells with in the vascular system at 4 dpf (Figure 4.9). However, GFP-labeled cells were not visible in unwounded *Tg(mpeg: eGFP)* embryos. This is also an expected observation, as the mpeg promoter is specific to macrophages, rather than monocytes, which would not be present in the absence of an inflammatory stimuli [35, 106].

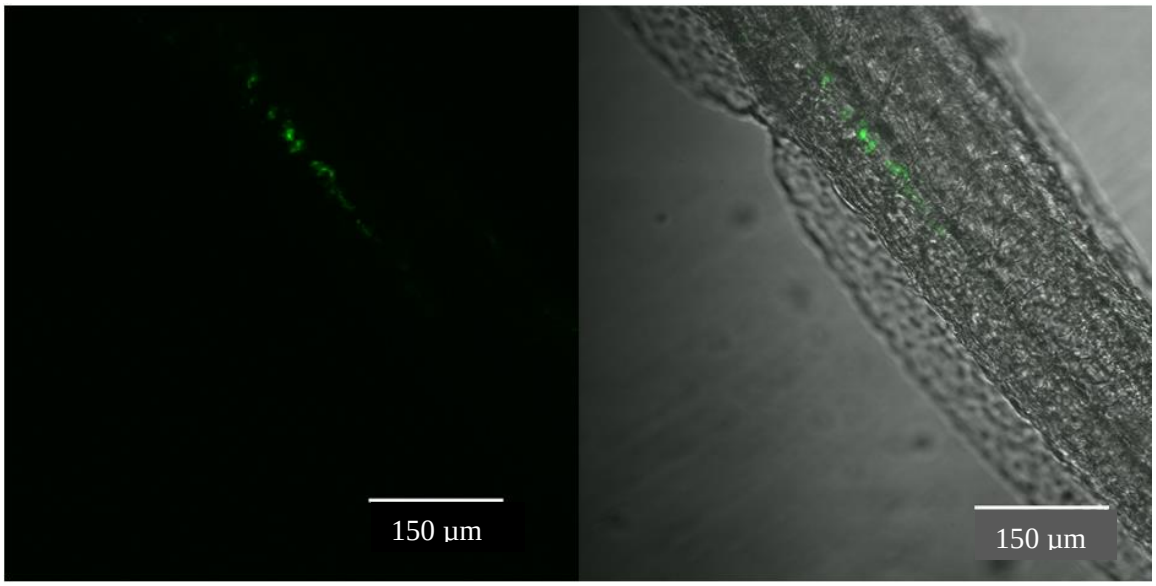

Figure 4.9: Confocal Image of *Tg(mpx: eGFP)* at 4 dpf. (Left) GFP image of neutrophils present in bloodstream of uninjured 4 dpf zebrafish embryo. (Right) overlay image of neutrophils (green) in bloodstream of 4 dpf embryo with transmitted light giving context to tissue location.

Preliminary injections of 25 µm Texas Red-labeled microparticles were performed in both transgenic strains. Microparticles of this size were selected due to improved success rates and ease of manipulation with the microinjection system compared to 50 µm and 10 µm microparticles, respectively.

The implanted biomaterials were easily detected post fixation, without any further modifications to the tissue. Two implanted microparticles were observed *in situ* 1 dpi within a 4 dpf *Tg(mpx: eGFP)* embryo using confocal microscopy (Figure 4.10). In addition, two GFP neutrophils were identified within the trunk tissue approximately 10 µm from the microparticle, suggesting these cells had exited circulation and were migrating towards the implant. However, this contrasts with other publications, in which significant neutrophil infiltration was observed at the surface of the microparticle at 1 dpi [30, 32]. However, our observations are quite preliminary, with only a single imaging series being taken for one implanted embryo.

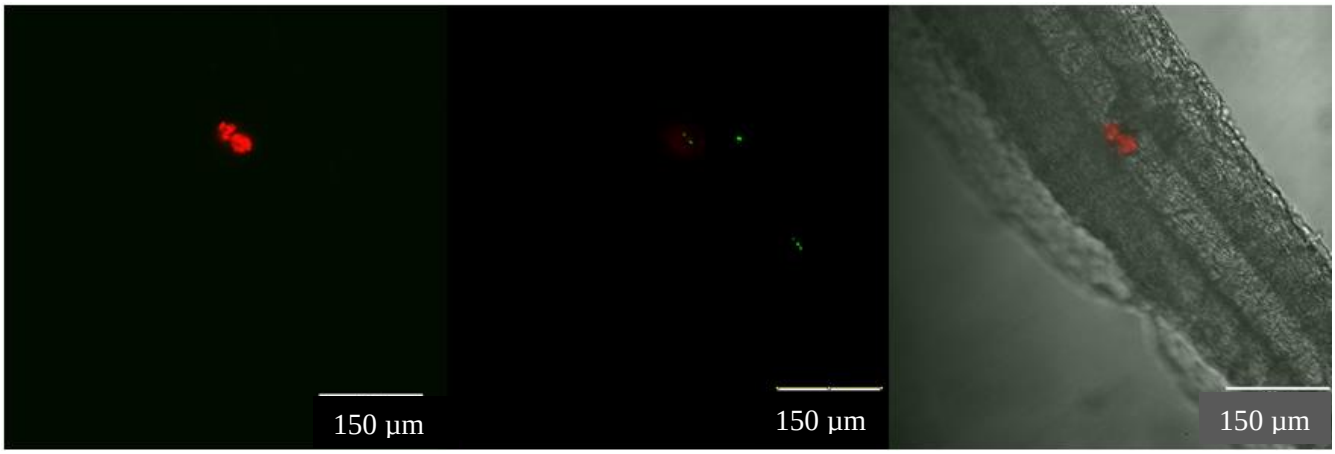

Figure 4.10: A confocal image series of a *Tg(mpx: eGFP)* embryo with 2 25 µm polyethylene microparticles (red) with neutrophils labelled in green 1 dpi. (Left) 2 microparticles embedded in the tissue of a 1 day post injection embryo. (Middle) a fluorescent overlay 10 µm deeper in the tissue from the microparticle with neutrophils in green. The signal in the GFP channel was enhanced to more clearly show the neutrophils. (Right) A transmitted overlay of the surrounding tissue of the embryo with microparticles visible.

However, injections of individual, 25 µm poly(ethylene) microparticles in the macrophage reporter strain clearly demonstrated an inflammatory response to the microparticle. Immediately post injection, there was a detectable presence of GFP-labelled macrophages in the tissues surrounding the implant site (Figure 4.11).

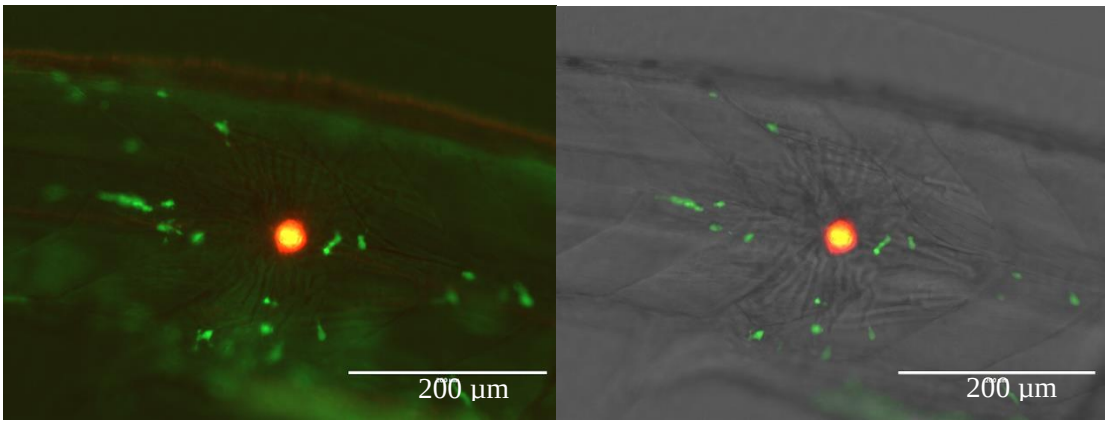

Figure 4.11: A 3 dpf *Tg(mpeg: eGFP)* embryo injected with a 25 µm Texas Red labelled poly(ethylene) microparticle. (Left) The microparticle (red) is embedded in the trunk of the zebrafish embryo, with macrophages (green) surrounding the site, with minimal infiltration at 30 minutes post injection. (Right) a 3-channel overlay with the previous fluorescent channels present, with a transmitted overlay to give context to the injection site.

While the macrophages were present around the wound site, there was low infiltration of macrophage in the area immediately around the microparticle. However, unlike current mammalian models, which demonstrate a slower macrophage accumulation, after 2 hpi, macrophage recruitment increased dramatically at the wound site (Figure 4.12). This early interrogation of the biomaterial surface agreed with the reported inflammation timelines in the recently published studies on microparticle implantation in zebrafish embryos [30, 32]. However, the injected embryos did not survive beyond 1 dpi, which limited our ability to compare the response in our model to what was reported in these two studies.

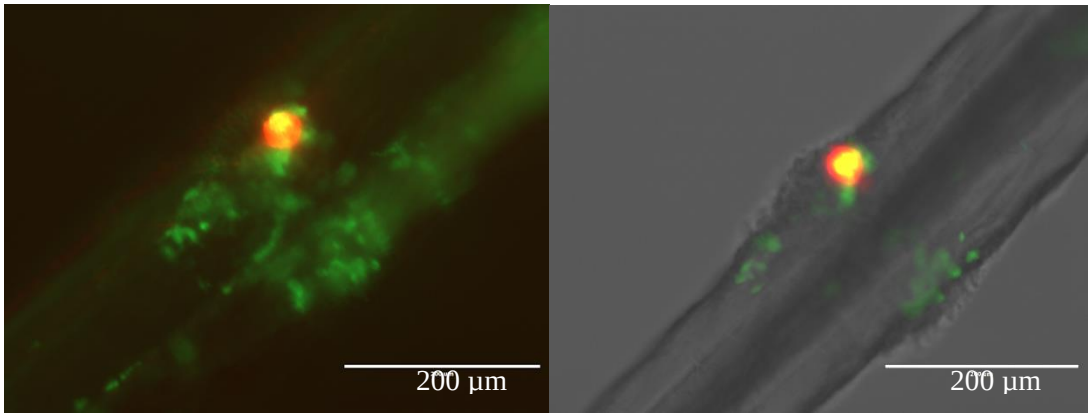

Figure 4.12: A 3 dpf *Tg(mpeg: eGFP)* embryo injected with a 25 µm Texas Red labelled poly(ethylene) microparticle. (Left) At 2 hpi, a large influx of macrophages (green) appear to be infiltrating the wound site and interrogating the surface of the microparticle (red). (Right) A 3-channel overlay with the previous fluorescent channels present, with a transmitted overlay added to give context to the injection site.

Both strains used in this study required a long adjustment period after shipping, and egg numbers were greatly reduced compared to their wildtype counterparts. This issue may have been caused by several factors, which include water quality in the static quarantine tanks, the advanced age of the received transgenic breeding stock, and potential environmental factors, such as fluctuation of room temperature and interruption of light cycle due to ongoing construction in the animal care facility [34, 72]. To address these issues, fish were kept quarantined as per the animal care protocol, but daily water exchanges were performed to maintain optimal water quality. Additionally, the initial batches of embryos produced from successful breeding were reserved for the sole purpose of colony expansion. As these new embryos are reared to breeding age, they are expected to provide a more consistent source of embryos than the older stock [34]. Finally, adjustments have been made within the colony room to decrease temperature and air flow fluctuations caused by building maintenance and renovation. With these changes, there has been a successfully established breeding stock of *Tg(mpx: eGFP)* for the

Queen's University zebrafish core. However, the age of the *Tg(mpeg: eGFP)* has proved challenging to overcome. When received, *Tg(mpeg: eGFP)* adults were 24 months old, 6 months past their ideal breeding age range [34]. Consequently, the limited viable embryos that were generated from this first generation of *Tg(mpeg: eGFP)* were reared in the colony to provide a second generation, which can be used as breeders once they reach adulthood.

4.5 Histological Analysis of Zebrafish Embryos

Histology and immunohistochemical techniques are frequently used to examine the host response in implant models, as they permit staining of tissues and cells while retaining information about the relative location and tissue structure surrounding the implant [16, 65]. However, due to the size and delicate nature of the zebrafish embryo tissue, histological assessment of zebrafish embryo tissue was technically challenging and specific histological techniques had to be developed for zebrafish embryos and larvae. First, a mold for generating embryo arrays was developed to enable processing of embryos using an automated processor, while keeping embryos organized and aligned. Then, fixation, sectioning and staining protocols for the embryo array were developed to improve the cohesion of the delicate embryonic tissue, which was easily disrupted or destroyed using conventional histology protocols.

4.5.1 Embryo Tissue Array

A master mold containing 50 imprint slots was 3D printed using a Miicraft 3D printer and clear resin BV-003 provided by the Escobedo group at Queen's University (Figure 4.13a). In addition to improving the quality of the processed tissue, the mold provided a more efficient histology process by allowing up to 50 embryos to be processed,

sectioned, and stained simultaneously. The master mold generated had high reusability with only simple washes in water necessary to remove residual agar before being used again, and can be stored at room temperature without the risk of deformation of the templates. As described in 3.5.1 this mold was used to generate an agar mold, which was then filled with embryos, covered with agar, and processed as a tissue block for histology using an automated processor (Figure 4.13b).

The agar mold retained all 50 templates after removal of the master mold, exhibited limited tearing and was pliable. After removal of the master mold, excess agar around the molded features was trimmed, leaving a raised lip around the templates to confine the agar overlay following embryo positioning within the wedge-shaped depressions (Figure 4.13c). The agar mold kept the embryos organized in an evenly spaced array and oriented along the same plane (Figure 4.13d).

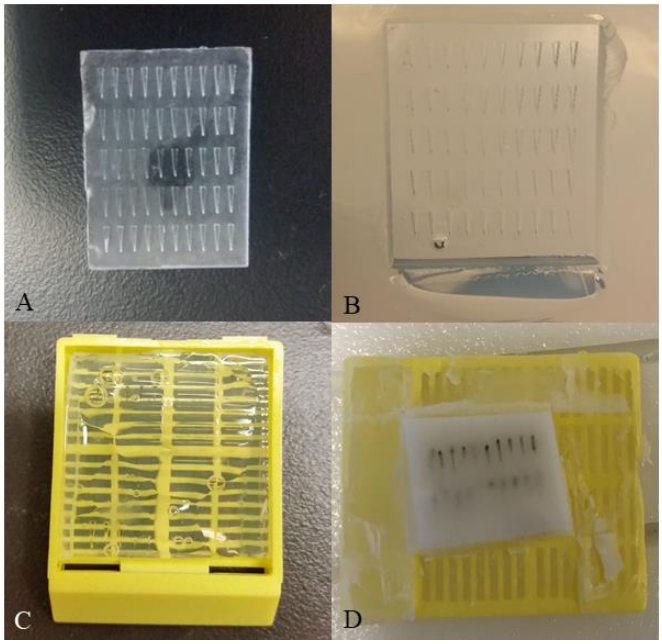

Figure 4.13: The workflow of the improved histology embedding process. A) The master mold 3D printed for embedding purposes. B) The pre-cut agar mold used for histology processing. C) An agar mold with fish present in the top left of the image, covered in agar. D) Post-paraffin embedding of the histology mold prior to sectioning.

Furthermore, it improved tissue cohesion during the processing stage, which is an important factor when examining tissue for damage caused by injections and implants.

4.5.2 Fixation protocol for zebrafish embryo and larvae

The intended application of histological and immunohistochemical analysis of zebrafish embryo and larvae was to examine cell recruitment around implants in wild-type fish, and differentiate between fibrous and non-fibrous tissues [65]. As such, hematoxylin and eosin (H&E) staining was used as a basic test stain, as it can highlight these key features [107]. However, while well established in other animal models, the ability to maintain tissue cohesion within embryos and larvae over the histological process was a significant challenge. Although agar embedding improved the tissue cohesion to a degree, there were issues with muscle fibers becoming torn or ripped during sectioning, which would prevent identification of implants or injection sites in the trunk of embryos in future studies (Figure 4.14a). Typically, tissues prepared for histology are first fixed in 10% formalin for up to 12 hours prior to processing and embedding in paraffin [65]. However, due to the small size of the embryos, it was determined that this resulted in "over-fixation" of the tissues, which causes the tissue to become brittle and causing subsequent damage in later stages of processing and staining. By reducing the fixation time, tissue cohesion within muscle fibers was vastly improved, with little to no tearing visible (Figure 4.14b).

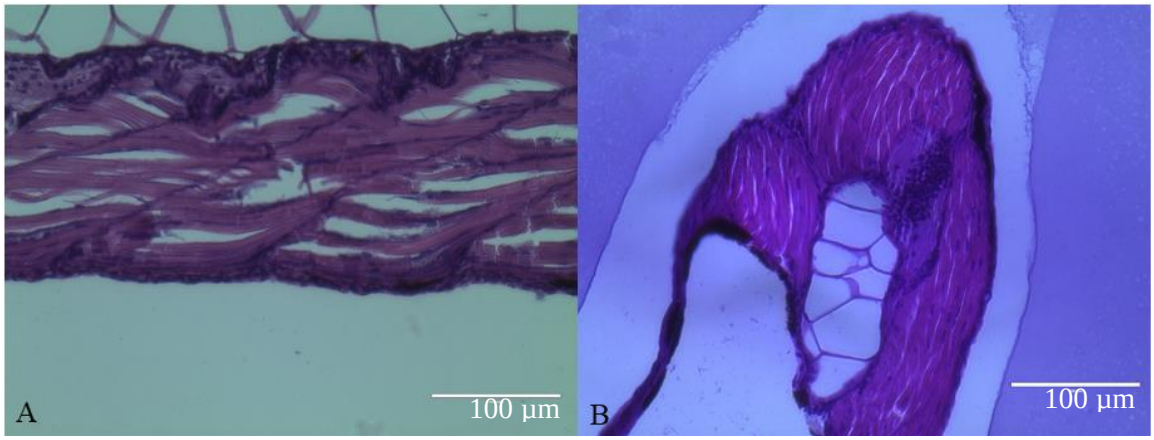

Figure 4.14: H&E staining of muscle tissue from the trunk of zebrafish larvae. A) Tissue fixed in formalin for 12 hours resulted in poor tissue cohesion. B) Muscle tissue of a larvae with a formalin fixation time of 2 hours yielded improve tissue cohesion that preserved the overall tissue structure to a greater extent that the extended 12 hour fixation.

In addition to improving the muscle fiber cohesion in sections of the trunk, this adjusted fixation time also proved delicate enough to allow for identification of the developing organs and tissues within the zebrafish embryos, including the rudimentary gut system, heart, brain and cartilage (Figure 4.15).

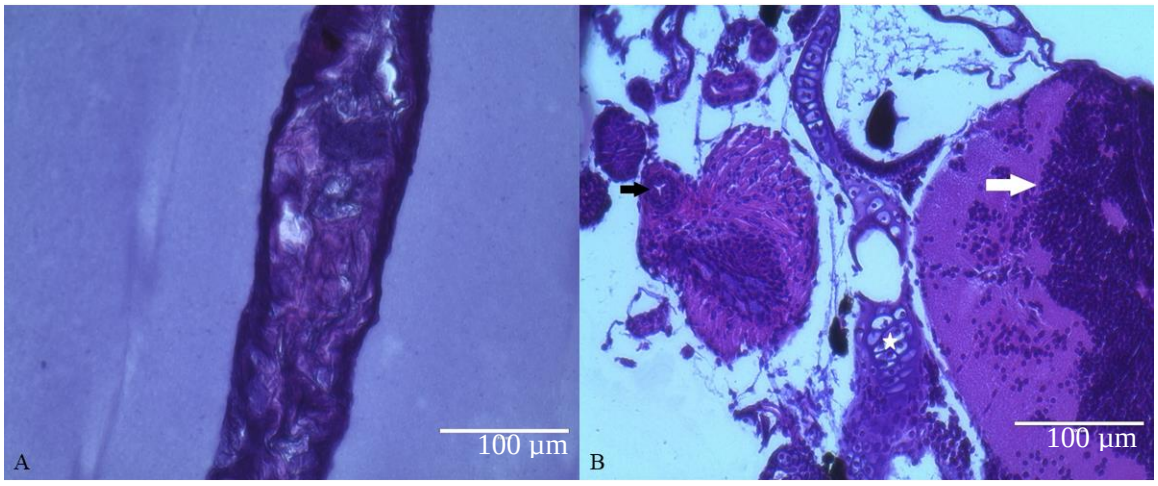

Figure 4.15: H&E staining of zebrafish larval tissue with agar embedding and reduced fixation times. A) The rudimentary gut system of a 12 dpf larva. Gut tissue is visible as the soft, disorganized tissue within the section. B) A section of a 14 dpf larva with preservation of delicate tissues, including a tricuspid heart valve (black arrow), developing brain (white arrow) and evidence of a developing skeletal system (white star), which is characterized by chondrocytes following the traditional jaw line of the zebrafish.

The ability to preserve the delicate structure of a tricuspid heart valve, as well as identifiable cell nuclei of chondrocytes, demonstrates the improvements of our histological methodology that will enable the histological evaluation of implant host responses in future studies.

Preliminary progress was also made in identifying wound sites and implants associated with injections (Figure 4.16). While only short-term examinations were possible due to poor microparticle retention, evidence of tissue damage was visible by H&E staining. H&E staining of injected larvae suggests that the wound site is identifiable at 9 dpi, as characterized by the disrupted tissue structure within the larvae's trunk (Figure 4.16a). The deformation along a pattern that is nearly perpendicular with surrounding tissue suggests a driving force that pulled tissue into a trench like formation. Followed by a "bulb" where the implantation occurred. The implant had been expelled in this embryo prior to fixation. Furthermore, the ability to clearly identify a 10 μm PS microparticle present within the tissue suggests that histological analysis can be performed on specimens that have implants within them (Figure 4.16b). The ability to identify the wound site at 9 dpi using histological techniques was significant, as Witherel *et al*. and Zhang *et al*. reported that injection sites are indistinguishable from surrounding tissue 3 dpi using confocal microscopy [30, 32].

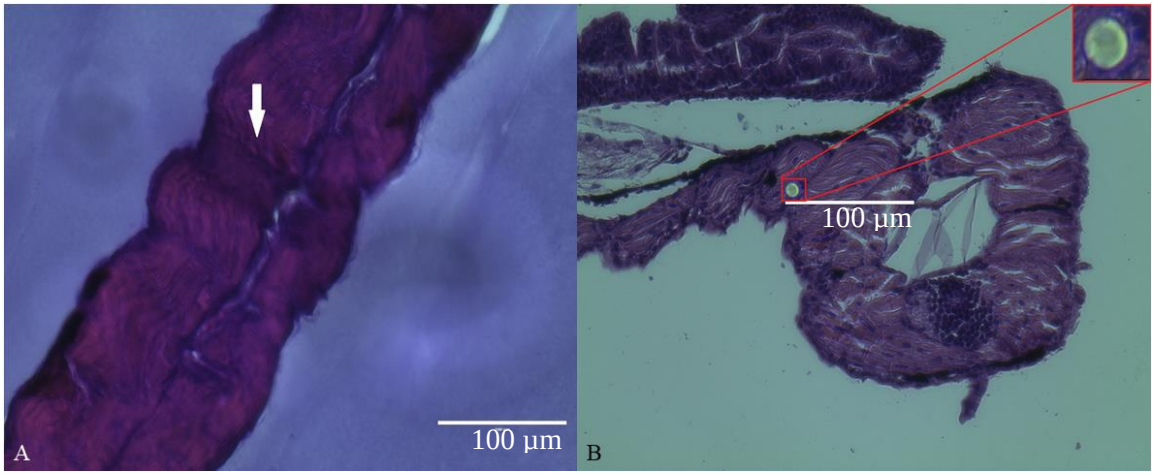

Figure 4.16: H&E staining of a zebrafish trunk following microparticle implantation. A) H&E section showing the injection site (white arrow) at 9 dpi. B) An example of a 10 µm poly(styrene) microparticle (red box; inset) embedded in the muscle tissue of a 1 dpi embryo.

The implant observed in Figure 4.16b appears to be surrounded by a thin ring of tissue with a different organization compared to oriented muscle tissue. While preliminary, this may suggest a host response specific to the surface of the biomaterial, rather than a generalized response to the injection. While confocal imaging of embryos provides a method of identifying cells around implants, histological assessment of specimens may be necessary for the identification of remodeling done post-injection.

4.6 Model Limitations

While developing the zebrafish embryo model, several limitations were identified. The most critical in evaluating the feasibility and appropriateness of using zebrafish embryos as animal models for biomaterial host responses are discussed here. Many of these limitations will be addressed in future work.

The first unexpected limitation was the poor retention of microparticles, which was observed particularly for larger implants. The two preliminary studies reporting on biomaterial implantation in zebrafish embryos did not address microparticle retention as a

potential issue when examining zebrafish host response [30, 32]. While Zhang *et al*. reported decreases in test groups over the course of their study, it was not identified if this was caused by mortality, or problems with microparticle retention [30].

Second, recent publications have highlighted the importance of the interaction between the adaptive and innate immune response for the development of FBR [11]. However, zebrafish do not exhibit a fully active adaptive immune system until 6 weeks post fertilization [69]. This lack of adaptive immunity could preclude the use of embryos to study the FBR. But, a fibrous capsule, a hallmark of the FBR, has been observed in adult zebrafish, which do have an adaptive immune response [32]. This suggests that adult zebrafish may be more appropriate than embryos for study of the FBR, rather than the embryo. However, the zebrafish embryo could provide a model of angiogenesis, and other regenerative functions that are not easily observable in other models [108].

Current work was also limited to injections performed with a manual microinjector. While this provides control of the number of implants per injection, there can be variability in injection volumes. This variability in volume may contribute to the mortality in zebrafish at early time points. Witherel *et al.* and Zhang *et al.* performed microparticle implantation using pneumatic injectors, which provide consistent injection volumes, but variable implant numbers [30, 32]. It was determined that the benefits of consistent implant numbers outweighed the potential variation injection volumes. Consistent implant numbers will enable the comparison of observed host-biomaterial interaction across injection groups. While excess injection volume is expected to rapidly diffuse from the wound site, it is possible that the variable injection volume may contribute to the reduced microparticle retention and viability of embryos. Consequently,

methods for standardizing injection volumes with the manual injector are currently being explored. Ideally, the manual and pneumatic injection methods should be evaluated head-to-head to determine which approach provides more control of experimental conditions, produces more reproducible data, and is more amenable to high-throughput techniques.

Chapter 5

Conclusions and Recommendations

5.1 Summary and Conclusions

The first aim of this thesis was to establish of a self-sustaining zebrafish colony at Queen's University. With over 200 wild-type breeding adults, there is a reliable source of embryos, and future work using this model can be carried out without risk of diminished colony viability. Furthermore, the initial development of two transgenic populations has been undertaken to provide the Fitzpatrick Lab with tools to examine neutrophil (*Tg(mpeg: eGFP)*) and macrophage (*Tg(mpx: eGFP)*) responses to various factors, such as biomaterial implants. Several challenges were observed with these transgenic strains, including a higher sensitivity to water quality compared to wildtype zebrafish. While establishing this colony, breeding protocols, water quality requirements, and life-stage appropriate diets were established, resulting in a well-equipped and trained animal care staff, who are now able to maintain zebrafish at all life cycle stages.

The second aim of this research was the establishment of experimental parameters for the implantation of individual microparticles in zebrafish embryos and larvae. Individual microparticles, as small as 10 µm, were successfully implanted via manual microinjection into the trunks of zebrafish embryo and larvae aged 3 to 5 days post fertilization (dpf). This specific age range was determined by observations in the development of recognizable structures and relevant systems, such as the innate immune system, pigmentation, and scales [31]. In addition to determining an appropriate age range for injection, needle pulling and beveling protocols were established for the generation of microneedles used with 10, 25, and 50 µm implants. Initial microneedle orifices were

targeted to be twice the diameter of the associated microparticle implant. Implantation success and retention, and zebrafish viability were assessed in wildtype zebrafish post injection using 10, 25, and 50 µm microparticles. Based on these results, it was determined that 10 µm implants, and wounds from needles with 20 µm bore sizes, were well tolerated by zebrafish. However, 25 µm implants and 50 µm needle bore sizes caused a significant decrease in viability compared to tricaine controls. While not statistically significant, there was also a notable decrease in viability in zebrafish embryos that received 25 µm implants, compared to their associated vehicle injections. 50 µm implants were not well tolerated by zebrafish, with no implanted animals surviving past 3 days post injection (dpi). Preliminary characterization of the transgenic *Tg(mpx: eGFP)* and *Tg(mpeg: eGFP)* strains was performed using fluorescence microscopy, including pilot microparticle implants. In both strains, early transparency was sufficient to allow tracking of fluorescently labelled macrophages and neutrophils in whole embryos. Furthermore, initial observations demonstrated a significant presence of macrophages within 1dpi at the wound site, and at the surface of the biomaterial, like recent publications [30, 32]. However, initial observations of neutrophil labelled transgenics did not demonstrate large numbers of neutrophils at the material surface, or wound site, at 1 dpi, in contradiction with current literature [30, 32].

The final aim of this research was to develop a protocol for histological analysis of the host-biomaterial response in zebrafish embryos. Initial attempts at processing and embedding resulted in tissues that were disorganized and hard to identify due to degradation. However, a 3D printed mold was generated, and used to form an agar tissue array template, which improved tissue cohesion. Furthermore, this mold improved

organization of the tissue, and lends itself to improving efficiency of histological analysis of future zebrafish studies. Additionally, formalin fixation times were examined to further improve tissue cohesion. By reducing the fixation time to two hours, tissue cohesion was vastly improved, and typically delicate structures were preserved and identified in histological sections.

5.2 Future Work and Recommendations

The work undertaken in this thesis provides a basis upon which future refinement and studies can occur. Reduction of the targeted bore size to the microparticle diameter ratio should be explored to determine if smaller bore sizes can reduce mortality while still injecting microparticles effectively. Improving microparticle retention, particularly for large microparticles, is essential for long term studies to be conducted with fewer total animals. Methods of improvement can include application of surgical adhesive to close the injection wound, or the use of a whisker tool to manipulate the microparticle deeper into the wound site, immediately post-injection [104]. Once the bore size ratio and retention problems have been addressed, survival curves should be repeated to assess limitations in implant size specifically, and how it relates to zebrafish viability in long term studies.

This work examined the use of a manual microinjector for the implantation of microparticles. While this provided control of the number of microparticles implanted per fish, it did not have precise control over injection volumes. Alternatively, pneumatic injectors provide precise volume control but can have variable implant numbers. Future work should develop a pneumatic injector system to examine the effect wound size has on the implantation process, while maintaining a constant injection volume. Furthermore,

in the development of a pneumatic system, different vehicles can be developed that could allow for the precise control of implantation numbers, such as polyvinylpyrrolidone with a molecular weight of 40,000 kDa (PVP 40) [30]. Additionally, a pneumatic injector lends itself to a high-throughput system, which would take advantage of the high fecundity of zebrafish [34]. As the platform is developed for high-throughput testing, advances in micro-scale fabrication can be used to build a microscale device for the incubation of individual zebrafish. Such a system could be generated from an optically transparent, oxygen permitting material such as polydimethylsiloxane (PDMS), which would allow zebrafish to be imaged rapidly and efficiently as they develop.

Once the injection parameters and techniques for implanting materials in embryos have been optimized, further use of transgenic strains of zebrafish should be done to examine how macrophage and neutrophils interact with the surface of implants.

In addition to continuing work with zebrafish embryos, recent publications have demonstrated a fibrous capsule around sutures in the trunk of adult zebrafish [32]. Future work on the zebrafish platform should assess the potential use of zebrafish adults as a model of foreign body reaction (FBR) to various implants. With developments in polymer science, research does not need to be limited to examination of sutures. Drug releasing implants, injectable polymer solutions, and others can be examined in an adult model to characterize the adult zebrafish host response to materials. Additionally, interactions between the adaptive and innate immune response, and how they relate to host-biomaterial interactions, can be examined in such a model due to the late development of adaptive immunity in zebrafish.

References

[1] P. M. Galletti, J. M. Anderson, D. I. Bardos, J. Black, G. S. Brody, L. Day, M. G. Duncanson, J. Grizzle, E. J. Kowalewski, K. Merritt *et al.*, "Clinical Application of Biomaterials," in *Consensus Development Conference*, 1982, vol. 4, no. 5, pp. 1-19.

[2] C. Sundback, T. Hadlock, M. Cheney, and J. Vacanti, "Manufacture of porous polymer nerve conduits by a novel low-pressure injection molding process," *Biomaterials,* vol. 24, no. 5, pp. 819-830, 2003.

[3] Z. X. Meng, Y. S. Wang, C. Ma, Y. F. Zheng, W. Zheng, and L. Li, "Electrospinning of PLGA/gelatin randomly-oriented and aligned nanofibers as potential scaffold in tissue engineering," *Materials Science & Engineering C,* vol. 30, no. 8, pp. 1204-1210, 2010.

[4] M. J. Moreno, A. Ajji, D. Mohebbi-Kalhori, M. Rukhlova, A. Hadjizadeh, and M. N. Bureau, "Development of a compliant and cytocompatible micro-fibrous polyethylene terephthalate vascular scaffold," *Journal of Biomedical Materials Research Part B: Applied Biomaterials,* vol. 97B, no. 2, pp. 201-214, 2011.

[5] L. Burton, D. Paget, N. B. Binder, K. Bohnert, B. J. Nestor, T. P. Sculco, L. Santambrogio, F. P. Ross, S. R. Goldring, and P. E. Purdue, "Orthopedic wear debris mediated inflammatory osteolysis is mediated in part by NALP3 inflammasome activation," *Journal of Orthopaedic Research,* vol. 31, no. 1, pp. 73-80, 2013.

[6] P. Liu, H. Yu, Y. Sun, M. Zhu, and Y. Duan, "A mPEG-PLGA-b-PLL copolymer carrier for adriamycin and siRNA delivery," *Biomaterials,* vol. 33, no. 17, pp. 4403-4412, 2012.

[7] A. K. McNally and J. M. Anderson, "Phenotypic expression in human monocyte-derived interleukin-4-induced foreign body giant cells and macrophages in vitro: Dependence on material surface properties," *Journal of Biomedical Materials Research Part A,* vol. 103, no. 4, pp. 1380-1390, 2015.

[8] N. Hiep and B.-T. Lee, "Electro-spinning of PLGA/PCL blends for tissue engineering and their biocompatibility," *Journal of Materials Science: Materials in Medicine,* vol. 21, no. 6, pp. 1969-1978, 2010.

[9] M. Barbeck, A. Motta, C. Migliaresi, R. Sader, C. Kirkpatrick, and S. Ghanaati, "Heterogeneity of biomaterial-induced multinucleated giant cells: possible importance for the regeneration process?," *Journal of Biomedical Materials Research,* 2015.

[10] J. M. Anderson, A. Rodriguez, and D. T. Chang, "Foreign body reaction to biomaterials," *Seminars in Immunology,* vol. 20, no. 2, pp. 86-100, 2008.

[11] J. C. Doloff, O. Veiseh, A. J. Vegas, H. H. Tam, S. Farah, M. Ma, J. Li, A. Bader, A. Chiu, A. Sadraei *et al.*, "Colony stimulating factor-1 receptor is a central component of the foreign body response to biomaterial implants in rodents and non-human primates," *Nat Mater,* Article vol. 16, no. 6, pp. 671-680, 2017.

[12] F. Alexis, "Factors affecting the degradation and drug-release mechanism of poly(lactic acid) and poly[(lactic acid)-co-(glycolic acid)]," *Polymer International,* vol. 54, no. 1, pp. 36-46, 2005.

[13] W. F. Liu, M. Ma, K. M. Bratlie, T. T. Dang, R. Langer, and D. G. Anderson, "Real-time in vivo detection of biomaterial-induced reactive oxygen species," *Biomaterials,* vol. 32, no. 7, pp. 1796-1801, 2011.

[14] Y. Wang, F. Papadimitrakopoulos, and D. J. Burgess, "Polymeric “smart” coatings to prevent foreign body response to implantable biosensors," *Journal of Controlled Release,* vol. 169, no. 3, pp. 341-347, 8/10/ 2013.

[15] E. J. Bergsma, F. R. Rozema, R. R. M. Bos, and W. C. D. Bruijn, "Foreign body reactions to resorbable poly(l-lactide) bone plates and screws used for the fixation of unstable zygomatic fractures," *Journal of Oral and Maxillofacial Surgery,* vol. 51, no. 6, pp. 666-670, 1993.

[16] J.-H. Ye, Y.-J. Xu, J. Gao, S.-G. Yan, J. Zhao, Q. Tu, J. Zhang, X.-J. Duan, C. A. Sommer, G. Mostoslavsky *et al.*, "Critical-size calvarial bone defects healing in a mouse model with silk scaffolds and SATB2-modified iPSCs," *Biomaterials,* vol. 32, no. 22, pp. 5065-5076, 2011.

[17] D. Akilbekova and K. M. Bratlie, "Quantitative Characterization of Collagen in the Fibrotic Capsule Surrounding Implanted Polymeric Microparticles through Second Harmonic Generation Imaging," *PLoS ONE,* vol. 10, no. 6, p. e0130386, 2015.

[18] J. M. Anderson and M. S. Shive, "Biodegradation and biocompatibility of PLA and PLGA microspheres," *Advanced Drug Delivery Reviews,* vol. 64, Supplement, no. 0, pp. 72-82, 2012.

[19] N. M. Biel, J. A. Lee, B. S. Sorg, and D. W. Siemann, "Limitations of the dorsal skinfold window chamber model in evaluating anti-angiogenic therapy during early phase of angiogenesis," *Vascular Cell,* journal article vol. 6, no. 1, p. 17, August 04 2014.

[20] J. N. Barbosa, P. Madureira, M. A. Barbosa, and A. P. Águas, "The influence of functional groups of self-assembled monolayers on fibrous capsule formation and cell recruitment," *Journal of Biomedical Materials Research Part A,* vol. 76A, no. 4, pp. 737-743, 2006.

[21] D. R. Yager and B. C. Nwomeh, "The proteolytic environment of chronic wounds," *Wound Repair and Regeneration,* vol. 7, no. 6, pp. 433-441, 1999.

[22] Y. Damestani, D. E. Galan-Hoffman, D. Ortiz, P. Cabrales, and G. Aguilar, "Inflammatory response to implantation of transparent nanocrystalline yttria-stabilized zirconia using a dorsal window chamber model," *Nanomedicine: Nanotechnology, Biology and Medicine,* vol. 12, no. 7, pp. 1757-1763, 2016.

[23] K. F. Hughes, M. D. Ries, and L. A. Pruitt, "Structural degradation of acrylic bone cements due to in vivo and simulated aging," *Journal of Biomedical Materials Research Part A,* vol. 65A, no. 2, pp. 126-135, 2003.

[24] C. M. Sayes, K. L. Reed, and D. B. Warheit, "Assessing Toxicity of Fine and Nanoparticles: Comparing In Vitro Measurements to In Vivo Pulmonary Toxicity Profiles," *Toxicological Sciences,* vol. 97, no. 1, pp. 163-180, 2007.

[25] C. M. Bennett, J. P. Kanki, J. Rhodes, T. X. Liu, B. H. Paw, M. W. Kieran, D. M. Langenau, A. Delahaye-Brown, L. I. Zon, M. D. Fleming *et al.*, "Myelopoiesis in the zebrafish, Danio rerio," *Blood,* 10.1182/blood.V98.3.643 vol. 98, no. 3, p. 643, 2001.

[26] J. N. Berman, J. P. Kanki, and A. T. Look, "Zebrafish as a model for myelopoiesis during embryogenesis," *Experimental Hematology,* vol. 33, no. 9, pp. 997-1006, 2005.

[27] M. Shah, D. M. Foreman, and M. W. Ferguson, "Neutralisation of TGF-beta 1 and TGF-beta 2 or exogenous addition of TGF-beta 3 to cutaneous rat wounds reduces scarring," *Journal of Cell Science,* vol. 108, no. 3, p. 985, 1995.

[28] C. Gray, C. A. Loynes, M. K. Whyte, D. C. Crossman, S. A. Renshaw, and T. J. Chico, "Simultaneous intravital imaging of macrophage and neutrophil behaviour during inflammation using a novel transgenic zebrafish," *Thrombosis and haemostasis,* vol. 105, no. 5, p. 811, 2011.

[29] J. M. Davis, H. Clay, J. L. Lewis, N. Ghori, P. Herbomel, and L. Ramakrishnan, "Real-Time Visualization of Mycobacterium-Macrophage Interactions Leading to Initiation of Granuloma Formation in Zebrafish Embryos," *Immunity,* vol. 17, no. 6, pp. 693-702, 2002.

[30] X. Zhang, O. W. Stockhammer, L. de Boer, N. O. E. Vischer, H. P. Spaink, D. W. Grijpma, and S. A. J. Zaat, "The zebrafish embryo as a model to quantify early inflammatory cell responses to biomaterials," *Journal of Biomedical Materials Research Part A,* pp. 2522-2532, 2017.

[31] C. B. Kimmel, W. W. Ballard, S. R. Kimmel, B. Ullmann, and T. F. Schilling, "Stages of embryonic development of the zebrafish," *Developmental Dynamics,* vol. 203, no. 3, pp. 253-310, 1995.

[32] C. E. Witherel, D. Gurevich, J. D. Collin, P. Martin, and K. L. Spiller, "Host–Biomaterial Interactions in Zebrafish," *American Chemical Society Biomaterials Science & Engineering,* 2017.

[33] R. M. White, A. Sessa, C. Burke, T. Bowman, J. LeBlanc, C. Ceol, C. Bourque, M. Dovey, W. Goessling, C. E. Burns *et al.*, "Transparent Adult Zebrafish as a Tool for In Vivo Transplantation Analysis," *Cell Stem Cell,* vol. 2, no. 2, pp. 183-189, 2008.

[34] A. Nasiadka and M. D. Clark, "Zebrafish breeding in the laboratory environment," *Institute for Laboratory Animal Research Journal,* vol. 53, no. 2, pp. 161-168, 2012.

[35] F. Ellett, L. Pase, J. W. Hayman, A. Andrianopoulos, and G. J. Lieschke, "mpeg1 promoter transgenes direct macrophage-lineage expression in zebrafish," *Blood,* vol. 117, no. 4, pp. e49-e56, 2011.

[36] E. A. Harvie and A. Huttenlocher, "Non-invasive Imaging of the Innate Immune Response in a Zebrafish Larval Model of Streptococcus iniae Infection," *Journal of visualized experiments : JoVE,* no. 98, p. e52788, 2015.

[37] W. Wang, X. Liu, D. Gelinas, B. Ciruna, and Y. Sun, "A fully automated robotic system for microinjection of zebrafish embryos," *PLoS one,* vol. 2, no. 9, p. e862, 2007.

[38] T. Takebe, N. Koike, S. Aoyama, Y. Adachi, H. Taniguchi, K. Sekine, M. Enomura, H. Koike, M. Kimura, T. Ogaeri *et al.*, "Vascularized and functional human liver from an iPSC-derived organ bud transplant," *NATURE,* vol. 499, no. 7459, pp. 481-481, 2013.

[39] N. Donoghoe, G. D. Rosson, and A. L. Dellon, "Reconstruction of the human median nerve in the forearm with the Neurotube™," *Microsurgery,* vol. 27, no. 7, pp. 595-600, 2007.

[40] J. C. Wright, "Critical Variables Associated with Nonbiodegradable Osmotically Controlled Implants," *The American Association of Pharmaceutical Scientists Journal,* vol. 12, no. 3, pp. 437-442, 2010.

[41] Y. Yang, N. Bajaj, P. Xu, K. Ohn, M. D. Tsifansky, and Y. Yeo, "Development of highly porous large PLGA microparticles for pulmonary drug delivery," *Biomaterials,* vol. 30, no. 10, pp. 1947-1953, 2009.

[42] F. H. Epstein, A. J. Singer, and R. A. Clark, "Cutaneous Wound Healing," *The New England Journal of Medicine,* vol. 341, no. 10, pp. 738-746, 1999.

[43] J. Sheehan, M. Templer, M. Gregory, R. Hanumanthaiah, D. Troyer, T. Phan, B. Thankavel, and P. Jagadeeswaran, "Demonstration of the extrinsic coagulation pathway in teleostei: Identification of zebrafish coagulation factor VII," *Proceedings of the National Academy of Sciences,* vol. 98, no. 15, pp. 8768-8773, 2001.

[44] E. W. Davie, K. Fujikawa, and W. Kisiel, "The coagulation cascade: initiation, maintenance, and regulation," *Biochemistry,* vol. 30, no. 43, pp. 10363-10370, 1991.

[45] S. Guo and L. A. DiPietro, "Critical Review in Oral Biology & Medicine: Factors Affecting Wound Healing," *Journal of Dental Research,* vol. 89, no. 3, pp. 219-229, 2010.

[46] C. F. Nathan, H. W. Murray, M. Wiebe, and B. Y. Rubin, "Identification of interferon-gamma as the lymphokine that activates human macrophage oxidative metabolism and antimicrobial activity," *Journal of Experimental Medicine,* vol. 158, no. 3, pp. 670-689, 1983.

[47] M. Stein, S. Keshav, N. Harris, and S. Gordon, "Interleukin 4 potently enhances murine macrophage mannose receptor activity: a marker of alternative immunologic macrophage activation," *The Journal of Experimental Medicine,* vol. 176, no. 1, pp. 287-292, 1992.

[48] A. G. Doyle, G. Herbein, L. J. Montaner, A. J. Minty, D. Caput, P. Ferrara, and S. Gordon, "Interleukin-13 alters the activation state of murine macrophages in vitro: Comparison with interleukin-4 and interferon-γ," *European journal of immunology,* vol. 24, no. 6, pp. 1441-1445, 1994.

[49] L. A. Brown, A. R. F. Rodaway, T. F. Schilling, T. Jowett, P. W. Ingham, R. K. Patient, and A. D. Sharrocks, "Insights into early vasculogenesis revealed by expression of the ETS-domain transcription factor Fli-1 in wild-type and mutant zebrafish embryos," *Mechanisms of Development,* vol. 90, no. 2, pp. 237-252, 2000.

[50] P. Pescatore, C. Verbeke, M. Härle, and B. C. Manegold, "Fibrin sealing in peptic ulcer bleeding: the fate of the clot," *Endoscopy,* vol. 30, no. 6, p. 519, 1998.

[51] E. A. Lenselink, "Role of fibronectin in normal wound healing," *International Wound Journal,* vol. 12, no. 3, pp. 313-316, 2015.

[52] P. Beauchamp, W. Moritz, J. M. Kelm, T. M. Ullrich, and C. Zuppinger, "Development and Characterization of a Scaffold-Free 3D Spheroid Model of Induced Pluripotent Stem Cell-Derived Human Cardiomyocytes," *Tissue Engineering Part C.,* vol. 21, no. 8, pp. 852-861, 2015.

[53] J. Morais, F. Papadimitrakopoulos, and D. Burgess, "Biomaterials/Tissue Interactions: Possible Solutions to Overcome Foreign Body Response," (in English), *The American Association of Pharmaceutical Scientists Journal,* vol. 12, no. 2, pp. 188-196, 2010/06/01 2010.

[54] D. W. Grainger, "All charged up about implanted biomaterials," *Nature Biotechnology,* News and Views vol. 31, no. 6, pp. 507-509, 2013.

[55] Y. Tabata and Y. Ikada, "Macrophage phagocytosis of biodegradable microspheres composed of L-lactic acid/glycolic acid homo-and copolymers," *Journal of biomedical materials research,* vol. 22, no. 10, pp. 837-858, 1988.

[56] K. M. DeFife, C. R. Jenney, E. Colton, and J. M. Anderson, "Cytoskeletal and adhesive structural polarizations accompany IL-13-induced human macrophage fusion," *Journal of Histochemistry & Cytochemistry,* vol. 47, no. 1, pp. 65-74, 1999.

[57] G. D. Marty and R. C. Summerfelt, "Pathways and Mechanisms for Expulsion of Surgically Implanted Dummy Transmitters from Channel Catfish," *Transactions of the American Fisheries Society,* vol. 115, no. 4, pp. 577-589, 1986.

[58] J. E. Sanders, S. D. Bale, and T. Neumann, "Tissue response to microfibers of different polymers: Polyester, polyethylene, polylactic acid, and polyurethane," *Journal of Biomedical Materials Research,* vol. 62, no. 2, pp. 222-227, 2002.

[59] J. E. Sanders, D. V. Cassisi, T. Neumann, S. L. Golledge, S. G. Zachariah, B. D. Ratner, and S. D. Bale, "Relative influence of polymer fiber diameter and surface charge on fibrous capsule thickness and vessel density for single-fiber implants," *Journal of Biomedical Materials Research Part A,* vol. 65A, no. 4, pp. 462-467, 2003.

[60] W. W. Jiang, S. H. Su, R. C. Eberhart, and L. Tang, "Phagocyte responses to degradable polymers," *Journal of Biomedical Materials Research Part A,* vol. 82A, no. 2, pp. 492-497, 2007.

[61] C. D. Williams, M. L. Bajt, M. R. Sharpe, M. R. McGill, A. Farhood, and H. Jaeschke, "Neutrophil activation during acetaminophen hepatotoxicity and repair in mice and humans," *Toxicology and Applied Pharmacology,* vol. 275, no. 2, pp. 122-133, 2014.

[62] E. Kunisch, R. Fuhrmann, A. Roth, R. Winter, W. Lungershausen, and R. W. Kinne, "Macrophage specificity of three anti-CD68 monoclonal antibodies (KP1, EBM11, and PGM1) widely used for immunohistochemistry and flow cytometry," *Annals of the rheumatic diseases,* vol. 63, no. 7, pp. 774-784, 2004.

[63] B. Krishnamoorthy, W. R. Critchley, J. B. Barnard, P. D. Waterworth, A. C. Caress, J. Fildes, and N. Yonan, "Validation of the endothelial staining markers CD31 and CD34 in

immunohistochemistry of the long saphenous vein," *Journal of cardiothoracic surgery,* vol. 10 Suppl 1, no. S1, p. A321, 2015.

[64] R. Jeffery, N. C. Direkze, S. Preston, T. Hunt, R. Poulsom, M. Alison, and N. A. Wright, "Techniques in development to prove the function of myofibroblasts transdifferentiated from whole bone marrow—Triple detection: Immunohistochemistry with in situ hybridisation for both DNA and RNA," *Gastroenterology,* vol. 124, no. 4, pp. A614-A615, 2003.

[65] A. L. Menke, J. M. Spitsbergen, A. P. Wolterbeek, and R. A. Woutersen, "Normal anatomy and histology of the adult zebrafish," *Toxicologic pathology,* vol. 39, no. 5, pp. 759-775, 2011.

[66] N. A. Sabaliauskas, C. A. Foutz, J. R. Mest, L. R. Budgeon, A. T. Sidor, J. A. Gershenson, S. B. Joshi, and K. C. Cheng, "High-throughput zebrafish histology," *Methods,* vol. 39, no. 3, pp. 246-254, 2006.

[67] C. B. Kimmel, S. K. Sessions, and R. J. Kimmel, "Radiosensitivity and time of origin of Mauthner neuron in the zebra fish," *Developmental Biology,* vol. 62, no. 2, pp. 526-529, 1978.

[68] J. Green, C. Collins, E. J. Kyzar, M. Pham, A. Roth, S. Gaikwad, J. Cachat, A. M. Stewart, S. Landsman, F. Grieco *et al.*, "Automated high-throughput neurophenotyping of zebrafish social behavior," *Journal of Neuroscience Methods,* vol. 210, no. 2, pp. 266-271, 9/30/ 2012.

[69] E. L. Benard, A. M. van der Sar, F. Ellett, G. J. Lieschke, H. P. Spaink, and A. H. Meijer, "Infection of Zebrafish Embryos with Intracellular Bacterial Pathogens," no. 61, p. e3781, 2012.

[70] S. A. Renshaw and N. S. Trede, "A model 450 million years in the making: zebrafish and vertebrate immunity," *Disease Models & Mechanisms,* vol. 5, no. 1, pp. 38-47, 2012.

[71] D. M. Parichy, M. R. Elizondo, M. G. Mills, T. N. Gordon, and R. E. Engeszer, "Normal Table of Post-Embryonic Zebrafish Development: Staging by Externally Visible Anatomy of the Living Fish," *Developmental dynamics : an official publication of the American Association of Anatomists,* vol. 238, no. 12, pp. 2975-3015, 2009.

[72] C. Lawrence, J. Best, A. James, and K. Maloney, "The effects of feeding frequency on growth and reproduction in zebrafish (Danio rerio)," *Aquaculture,* vol. 368–369, pp. 103-108, 2012.

[73] S. H. Lam, H. L. Chua, Z. Gong, T. J. Lam, and Y. M. Sin, "Development and maturation of the immune system in zebrafish, Danio rerio: a gene expression profiling, in situ hybridization and immunological study," *Developmental and Comparative Immunology,* vol. 28, no. 1, pp. 9-28, 2004.

[74] N. G. Holtzman, M. K. Iovine, J. O. Liang, and J. Morris, "Learning to Fish with Genetics: A Primer on the Vertebrate Model *Danio rerio*," *Genetics,* 10.1534/genetics.116.190843 vol. 203, no. 3, p. 1069, 2016.

[75] Y. Bradford, T. Conlin, N. Dunn, D. Fashena, K. Frazer, D. G. Howe, J. Knight, P. Mani, R. Martin, S. A. Moxon *et al.*, *ZFIN: enhancements and updates to the zebrafish model organism database*. 2011.

[76] J. Krauss, P. Astrinides, H. G. Frohnhöfer, B. Walderich, and C. Nüsslein-Volhard, "transparent, a gene affecting stripe formation in Zebrafish, encodes the mitochondrial protein Mpv17 that is required for iridophore survival," *Biology Open,* 10.1242/bio.20135132 vol. 2, no. 7, p. 703, 2013.

[77] J. R. Mathias, M. E. Dodd, K. B. Walters, S. K. Yoo, E. A. Ranheim, and A. Huttenlocher, "Characterization of zebrafish larval inflammatory macrophages," *Developmental and Comparative Immunology,* vol. 33, no. 11, pp. 1212-1217, 2009.

[78] G. M. Her, C.-C. Chiang, W.-Y. Chen, and J.-L. Wu, "In vivo studies of liver-type fatty acid binding protein (L-FABP) gene expression in liver of transgenic zebrafish (Danio rerio)," *Federation of European Biochemical Societies letters,* vol. 538, no. 1-3, pp. 125-133, 2003.
[79] A. J. Davidson and L. I. Zon, "The *definitive* (and *primitive*) guide to zebrafish hematopoiesis," *Oncogene,* vol. 23, no. 43, pp. 7233-7246, 2004.
[80] L. Cao, A. Wu, and G. A. Truskey, "Biomechanical effects of flow and coculture on human aortic and cord blood-derived endothelial cells," *Journal of Biomechanics,* vol. 44, no. 11, pp. 2150-2157, 2011.
[81] N. D. Lawson and B. M. Weinstein, "In Vivo Imaging of Embryonic Vascular Development Using Transgenic Zebrafish," *Developmental Biology,* vol. 248, no. 2, pp. 307-318, 2002.
[82] R. Carvalho, J. de Sonneville, O. W. Stockhammer, N. D. L. Savage, W. J. Veneman, T. H. M. Ottenhoff, R. P. Dirks, A. H. Meijer, and H. P. Spaink, "A High-Throughput Screen for Tuberculosis Progression," *PLoS ONE,* vol. 6, no. 2, p. e16779, 2011.
[83] C. Sullivan and C. H. Kim, "Zebrafish as a model for infectious disease and immune function," *Fish and Shellfish Immunology,* vol. 25, no. 4, pp. 341-350, 2008.
[84] T. R. Frieden, T. R. Sterling, S. S. Munsiff, C. J. Watt, and C. Dye, "Tuberculosis," *The Lancet,* vol. 362, no. 9387, pp. 887-899, 2003.
[85] I. Rosenkrands, R. A. Slayden, J. Crawford, C. Aagaard, B. E. I. Clifton, and P. Andersen, "Hypoxic Response of Mycobacterium tuberculosis Studied by Metabolic Labeling and Proteome Analysis of Cellular and Extracellular Proteins," *Journal of Bacteriology,* vol. 184, no. 13, pp. 3485-3491, 2002.
[86] J. S. Blackburn, M. S. Ignatius, D. M. Langenau, S. Liu, A. R. Raimondi, and C. D. Salthouse, "High-throughput imaging of adult fluorescent zebrafish with an LED fluorescence macroscope," (in English), *Nature Protocols,* Report vol. 6, p. 229+, 2011.
[87] H. P. Spaink, C. Cui, M. I. Wiweger, H. J. Jansen, W. J. Veneman, R. Marín-Juez, J. de Sonneville, A. Ordas, V. Torraca, W. van der Ent *et al.*, "Robotic injection of zebrafish embryos for high-throughput screening in disease models," *Methods,* vol. 62, no. 3, pp. 246-254, 2013.
[88] W. J. Veneman, O. W. Stockhammer, L. De Boer, S. A. Zaat, A. H. Meijer, and H. P. Spaink, "A zebrafish high throughput screening system used for Staphylococcus epidermidis infection marker discovery," *BioMed Central Genomics,* vol. 14, no. 1, p. 255, 2013.
[89] Y. C. G. J. Paquay, J. E. de Ruijter, J. P. C. M. van der Waerden, and J. A. Jansen, "Tissue reaction to Dacron® velour and titanium fibre mesh used for anchorage of percutaneous devices," *Biomaterials,* vol. 17, no. 12, pp. 1251-1256, 1996.
[90] S. Kumar and S. B. Hedges, "A molecular timescale for vertebrate evolution," *Nature,* vol. 392, pp. 917-920, 1998.
[91] A. M. Wolf, D. Wolf, H. Rumpold, B. Enrich, and H. Tilg, "Adiponectin induces the anti-inflammatory cytokines IL-10 and IL-1RA in human leukocytes," *Biochemical and biophysical research communications,* vol. 323, no. 2, pp. 630-635, 2004.
[92] M. V. Vellayappan, S. K. Jaganathan, and I. I. Muhamad, "Unravelling the potential of nitric acid as a surface modifier for improving the hemocompatibility of metallocene polyethylene for blood contacting devices," *PeerJ,* vol. 4, p. e1388, 2016.
[93] E. Cenni, C. R. Arciola, G. Ciapetti, D. Granchi, L. Savarino, S. Stea, D. Cavedagna, A. Pizzoferrato, T. Curti, and G. Falsone, "Platelet and coagulation factor variations induced in vitro by polyethylene terephthalate (Dacron®) coated with pyrolytic carbon," *Biomaterials,* vol. 16, no. 13, pp. 973-976, 1995.

[94] C. A. Toumbis, J. L. Kronick, P. H. Wooley, and S. Nasser, "Total joint arthroplasty and the immune response," *Seminars in Arthritis and Rheumatism,* vol. 27, no. 1, pp. 44-47, 1997.
[95] M. U. Amin, G. Scott, and L. M. K. Tillekeratne, "Mechanism of the photo initiation process in polyethylene," *European Polymer Journal,* vol. 11, 1975.
[96] C. H. Bamford and R. P. Wayne, "Polymerization in the solid phase: A polycondensation reaction," *Polymer,* vol. 10, pp. 661-681, 1969.
[97] A. Hussain, B. Curry, L. Cahalan, S. Minkin, M. Gartner, and P. Cahalan, "Development and in vitro evaluation of infection resistant materials: A novel surface modification process for silicone and Dacron," *Journal of biomaterials applications,* vol. 30, no. 7, p. 1103, 2016.
[98] B. D. Ratner, A. S. Hoffman, F. J. Schoen, and J. E. Lemons, *Biomaterials science: an introduction to materials in medicine*. Academic press, 2004.
[99] N. Muhammad, N. Kryuchkova, T. Dworeck, F. Rodríguez-Ropero, and M. Fioroni, "Enhanced EGFP Fluorescence Emission in Presence of PEG Aqueous Solutions and--Copolymer Vesicles," *BioMed research international,* vol. 2013, 2013.
[100] S. Omelon, J. Georgiou, and W. Habraken, "A cautionary (spectral) tail: red-shifted fluorescence by DAPI–DAPI interactions," *Biochemical Society Transactions,* 10.1042/BST20150231 vol. 44, no. 1, p. 46, 2016.
[101] F. Bestvater, E. Spiess, G. Stobrawa, M. Hacker, T. Feurer, T. Porwol, U. Berchner-Pfannschmidt, C. Wotzlaw, and H. Acker, "Two-photon fluorescence absorption and emission spectra of dyes relevant for cell imaging," *Journal of Microscopy,* vol. 208, no. 2, pp. 108-115, 2002.
[102] H. Gelb, H. Ralph Schumacher, J. Cuckler, and D. G. Baker, "In vivo inflammatory response to polymethylmethacrylate particulate debris: Effect of size, morphology, and surface area," *Journal of Orthopaedic Research,* vol. 12, no. 1, pp. 83-92, 1994.
[103] J. L. Strykowski and J. M. Schech, "Effectiveness of Recommended Euthanasia Methods in Larval Zebrafish (*Danio rerio*)," *Journal of the American Association for Laboratory Animal Science,* vol. 54, no. 1, pp. 81-84, 2015.
[104] G. F. Gerlach, E. E. Morales, and R. A. Wingert, "Microbead Implantation in the Zebrafish Embryo," *Journal of Visualized Experiments : JoVE,* no. 101, p. 52943, 2015.
[105] B. Fraysse, R. Mons, and J. Garric, "Development of a zebrafish 4-day embryo-larval bioassay to assess toxicity of chemicals," *Ecotoxicology and Environmental Safety*, vol. 63, no. 2, pp. 253-267, 2006.
[106] A. Zakrzewska, C. Cui, O. W. Stockhammer, E. L. Benard, H. P. Spaink, and A. H. Meijer, "Macrophage-specific gene functions in Spi1-directed innate immunity," *Blood,* vol. 116, no. 3, pp. e1-e11, 2010.
[107] J. Sullivan-Brown, M. E. Bisher, and R. D. Burdine, "Embedding, Serial Sectioning and Staining of Zebrafish Embryos Using JB-4™ Resin," *Nature protocols,* vol. 6, no. 1, pp. 46-55, 2011.
[108] M. Gemberling, T. J. Bailey, D. R. Hyde, and K. D. Poss, "The zebrafish as a model for complex tissue regeneration," *Trends in genetics : TIG,* vol. 29, no. 11, p. 10.1016/j.tig.2013.07.003, 2013.

Appendix A

Table A.1: Pulling parameters A, B, and C, for the WPI PUL-1000 microneedle pulling machine. Heat represents the current passed through the microfilament and can range from 0 – 999, depending on the glass capillaries being used. Force is a measure of the force delivered to the carriage by the solenoid and has arbitrary units ranging from 50 – 400g. Distance is the desired extension per step measured in mm; a minimum of 3.5 mm is required to cause separation of the microcapillary. Delay is the time between steps, which affects the amount the capillary can cool prior to heating.

Program	Step	Heat	Force (g)	Distance (mm)	Delay (ms)
A	1	550	150	2.00	25
	2	450	170	1.00	40
	3	300	200	0.50	20
	4	200	100	0.50	20
B	1	550	150	1.60	35
	2	425	200	0.9	50
	3	300	200	0.4	20
	4	250	130	0.4	20
C	1	600	200	2.00	10
	2	550	200	1.00	10
	3	550	200	1.00	0